

Important Notice to Authors

Attached is a PDF proof of your forthcoming article in *Physical Review D*. The article accession code is DX11765.

Please note that as part of the production process, APS converts all articles, regardless of their original source, into standardized XML that in turn is used to create the PDF and online versions of the article as well as to populate third-party systems such as Portico, Crossref, and Web of Science. We share our authors' high expectations for the fidelity of the conversion into XML and for the accuracy and appearance of the final, formatted PDF. This process works exceptionally well for the vast majority of articles; however, please check carefully all key elements of your PDF proof, particularly any equations or tables.

Figures submitted electronically as separate PostScript files containing color appear in color in the online journal. However, all figures will appear as grayscale images in the print journal unless the color figure charges have been paid in advance, in accordance with our policy for color in print (<http://journals.aps.org/authors/color-figures-print>).

No further publication processing will occur until we receive your response to this proof.

Specific Questions and Comments to Address for This Paper

The numbered items below correspond to numbers in the margin of the proof pages pinpointing the source of the question and/or comment. The numbers will be removed from the margins prior to publication.

Q: Please check that all references include complete titles.

- 1 Second proof: Please carefully confirm that all first-proof corrections were addressed and that changes were made accurately.
- 2 Second proof: Please confirm the paper is now ready to be published in its current form.
- 3 Second proof: Please check the updated author affiliations are correct?
- 4 Second proof: In terms 'nontidal', 'mass gap', 'subdominant', 'multidimensional', 'postmerger', 'cosampled', 'subpercent' hyphens can not be restored. Hyphens are used only for the adjectival usage as per PRD style guidelines, so the requested correction could not be made.
- 5 Second proof: Please note that Refs. [3] and [4] are same references we removed [3] and renumbered the references.

Titles in References

The editors now encourage insertion of article titles in references to journal articles and e-prints. This format is optional, but if chosen, authors should provide titles for *all* eligible references. If article titles remain missing from eligible references, the production team will remove the existing titles at final proof stage.

Funding Information

Information about an article's funding sources is now submitted to Crossref to help you comply with current or future funding agency mandates. Crossref's Open Funder Registry (<http://www.crossref.org/fundingdata/>) is the definitive registry of funding agencies. Please ensure that your acknowledgments include all sources of funding for your article following any requirements of your funding sources. Where possible, please include grant and award ids. Please carefully check the following funder information we have already extracted from your article and ensure its accuracy and completeness:

- Natural Sciences and Engineering Research Council of Canada, FundRef ID <http://dx.doi.org/10.13039/501100000038> (Canada)
- Ontario MINISTRY OF ECONOMIC DEVELOPMENT AND INNOVATION, FundRef ID <http://dx.doi.org/10.13039/501100000192> (Canada/Ontario)

- Canada Research Chairs, FundRef ID <http://dx.doi.org/10.13039/501100001804> (Canada/Ontario)
- Canadian Institute for Advanced Research, FundRef ID <http://dx.doi.org/10.13039/100007631> (Canada/Ontario)

Other Items to Check

- Please note that the original manuscript has been converted to XML prior to the creation of the PDF proof, as described above. Please carefully check all key elements of the paper, particularly the equations and tabular data.
- Title: Please check; be mindful that the title may have been changed during the peer review process.
- Author list: Please make sure all authors are presented, in the appropriate order, and that all names are spelled correctly.
- Please make sure you have inserted a byline footnote containing the email address for the corresponding author, if desired. Please note that this is not inserted automatically by this journal.
- Affiliations: Please check to be sure the institution names are spelled correctly and attributed to the appropriate author(s).
- Receipt date: Please confirm accuracy.
- Acknowledgments: Please be sure to appropriately acknowledge all funding sources.
- References: Please check to ensure that titles are given as appropriate.
- Hyphenation: Please note hyphens may have been inserted in word pairs that function as adjectives when they occur before a noun, as in “x-ray diffraction,” “4-mm-long gas cell,” and “R-matrix theory.” However, hyphens are deleted from word pairs when they are not used as adjectives before nouns, as in “emission by x rays,” “was 4 mm in length,” and “the R matrix is tested.”
Note also that Physical Review follows U.S. English guidelines in that hyphens are not used after prefixes or before suffixes: superresolution, quasiequilibrium, nanoprecipitates, resonancelike, clockwise.
- Please check that your figures are accurate and sized properly. Make sure all labeling is sufficiently legible. Figure quality in this proof is representative of the quality to be used in the online journal. To achieve manageable file size for online delivery, some compression and downsampling of figures may have occurred. Fine details may have become somewhat fuzzy, especially in color figures. The print journal uses files of higher resolution and therefore details may be sharper in print. Figures to be published in color online will appear in color on these proofs if viewed on a color monitor or printed on a color printer.
- Overall, please proofread the entire *formatted* article very carefully. The redlined PDF should be used as a guide to see changes that were made during copyediting. However, note that some changes to math and/or layout may not be indicated.

Ways to Respond

- **Web:** If you accessed this proof online, follow the instructions on the web page to submit corrections.
- **Email:** Send corrections to aps-robot@luminad.com. Include the accession code DX11765 in the subject line.
- **Fax:** Return this proof with corrections to +1.855.808.3897.

If You Need to Call Us

You may leave a voicemail message at +1.855.808.3897. Please reference the accession code and the first author of your article in your voicemail message. We will respond to you via email.

Measuring neutron star tidal deformability with Advanced LIGO: A Bayesian analysis of neutron star-black hole binary observations

Prayush Kumar,^{1,*} Michael Pürrer,² and Harald P. Pfeiffer^{1,3,2}

¹*Canadian Institute for Theoretical Astrophysics, University of Toronto,
Toronto M5S 3H8, Canada*

²*Max Planck Institute for Gravitational Physics (Albert Einstein Institute),
Am Mühlenberg 1, Potsdam-Golm 14476, Germany*

³*Canadian Institute for Advanced Research, Toronto M5G 1Z8, Canada*
(Received 20 October 2016)

The pioneering discovery of gravitational waves (GWs) by Advanced LIGO has ushered us into an era of observational GW astrophysics. Compact binaries remain the primary target sources for GW observation, of which neutron star-black hole (NSBH) binaries form an important subset. GWs from NSBH sources carry signatures of (a) the tidal distortion of the neutron star by its companion black hole during inspiral, and (b) its potential tidal disruption near merger. In this paper, we present a Bayesian study of the measurability of neutron star tidal deformability $\Lambda_{\text{NS}} \propto (R/M)_{\text{NS}}^5$ using observation(s) of inspiral-merger GW signals from disruptive NSBH coalescences, taking into account the crucial effect of black hole spins. First, we find that if nontidal templates are used to estimate source parameters for an NSBH signal, the bias introduced in the estimation of nontidal physical parameters will only be significant for loud signals with signal-to-noise ratios greater than ≈ 30 . For similarly loud signals, we also find that we can begin to put interesting constraints on Λ_{NS} (factor of 1–2) with individual observations. Next, we study how a population of realistic NSBH detections will improve our measurement of neutron star tidal deformability. For an astrophysically likely population of *disruptive* NSBH coalescences, we find that 20–35 events are sufficient to constrain Λ_{NS} within $\pm 25\%–50\%$, depending on the neutron star equation of state. For these calculations we assume that LIGO will detect black holes with masses within the astrophysical *mass gap*. In case the mass gap remains *preserved* in NSBHs detected by LIGO, we estimate that approximately 25% additional detections will furnish comparable Λ_{NS} measurement accuracy. In both cases, we find that it is the loudest 5–10 events that provide most of the tidal information, and not the combination of tens of low-SNR events, thereby facilitating targeted numerical-GR follow-ups of NSBHs. We find these results encouraging, and recommend that an effort to measure Λ_{NS} be planned for upcoming NSBH observations with the LIGO-Virgo instruments.

DOI:

I. INTRODUCTION

The Advanced LIGO (aLIGO) observatories completed their first observing run “O1” early in 2016, operating at a factor of 3–4 higher gravitational-wave (GW) strain sensitivity than their first-generation counterparts [1]. During O1, they made the first direct observation of gravitational waves [2]. Emitted by a pair of coalescing black holes, these waves heralded an era of observational GW astrophysics as they traveled through Earth. Towards the end of this decade, we expect aLIGO to reach its design sensitivity. In addition to the U.S.-based efforts, we also expect the French-Italian detector Advanced Virgo [3], Japanese detector KAGRA [4,5], and LIGO-India [6] to begin observing at comparable sensitivities within a few years. With a global network of sensitive GW observatories, we can expect GW astronomy to face significant developments over the coming years.

Coalescing compact binaries of stellar-mass black holes (BH) and/or neutron stars (NS) are the primary targets for the second generation GW detectors [7–18]. A binary system of black holes was recently observed by aLIGO [2]. Previously, stellar-mass black holes had only been observed by inference in mixed binaries with stellar companion (through electromagnetic observations of the companion) [19–21]. Neutron stars, on the other hand, have had numerous sightings. Thousands of electromagnetically emitting neutron stars, or pulsars, have been documented [22], in varied situations: as radio pulsars [22,23], in binary systems with a stellar companion [22–25], and in binary neutron stars (BNSs) [22,23,26–28]. Mixed binaries of black holes and neutron stars are an astrophysically interesting class of systems [15,16,29,30], which has not yet been detected. We expect to observe $\mathcal{O}(10)$ mixed binaries per year with aLIGO [31].

Neutron star-black hole (NSBH) binaries are of interest for multiple reasons. For instance, they have been long associated with (as possible progenitors of) short

*prkumar@cita.utoronto.ca

69 gamma-ray bursts (SGRBs) [32–40]. Depending on their
 70 equation of state (EoS), NSs can get disrupted by the tidal
 71 field of their companion BHs. Once disrupted, most of the
 72 NS material falls into the hole over an $\mathcal{O}(1 \text{ ms})$ time scale,
 73 with the rest partly getting ejected as unbound material and
 74 partly forming an accretion disk around the BH. This
 75 short lived ($0.1 - 1 \text{ s}$) disk-BH system is hypothesized to
 76 drive SGRBs through the production of relativistic jets
 77 [38,39,41–44]. However, whether or not such a system
 78 forms depends also on the nature of the BH. Massive BHs
 79 (with $m_{\text{BH}} \gtrsim 12 M_{\odot}$), as well as BHs with large retrograde
 80 spins, tend to swallow the NS whole without forming
 81 a disk [45]. On the other hand, *low-mass* BHs with
 82 $m_{\text{BH}} \in [3 M_{\odot}, 12 M_{\odot}]$,¹ can disrupt their companion NSs
 83 much before merger, forming long-sustained disks that are
 84 required to sustain SGRBs [42,46–49]. A *coincident* detec-
 85 tion of both GWs and gamma rays from an NSBH merger
 86 will provide us with a unique opportunity to confirm this
 87 hypothesized link between NSBH mergers and GRBs [50].

88 Another question that compact object mergers can help
 89 answer is “what is the nature of matter at nuclear densities
 90 supported by NS”? A large fraction of the past work aimed
 91 at measuring NS matter effects from GW signals has
 92 consisted of inquiries about BNSs [51–62]. In this paper,
 93 we will instead focus on NSBHs. During the course of early
 94 inspiral, the tidal field of the BH produces a deformation in
 95 its companion NS. The quadrupolar moment of the star
 96 associated with this deformation also depends on its
 97 material properties, through an EoS-dependent tidal
 98 deformability parameter Λ_{NS} . This induced quadrupolar
 99 moment changes over the orbital time scale, resulting in the
 100 emission of GWs in *coherence* with the orbital waves.
 101 These waves draw more energy from the orbit and increase
 102 the inspiral rate [as compared to an equivalent binary black
 103 hole (BBH)] [63]. Closer to merger, the strong tidal field of
 104 the BH can disrupt the NS. The quadrupolar moment of the
 105 disrupted binary system falls monotonically over a milli-
 106 second time scale [41,42,64–66], resulting in the damping
 107 of GW amplitude. This penultimate stage also depends
 108 strongly on the internal structure and energy transport
 109 mechanism of the NS, and carries the strongest tidal
 110 signature in the GW spectrum [43,46].

111 Gravitational waves emitted by coalescing NSBH binaries
 112 carry subtle hints of the NS EoS from inspiral through
 113 to merger. During early inspiral, the tidal dephasing is
 114 relatively weak and has a frequency dependence equivalent
 115 to a fifth Post-Newtonian (PN) order effect [67]. Closer to
 116 merger, a disruptive fate of the NS can result in a strong
 117 suppression of GW emission above a cutoff frequency [66].
 118 Some past studies of tidal measurements with NSBH
 119 binaries have used PN inspiral-only waveforms [68]. In

120 doing so, however, they ignore (i) the merger signal which
 121 could contain significant information for NSBHs, and
 122 (ii) the errors due to unknown vacuum terms in PN
 123 waveforms, which could dominate over the tidal terms
 124 themselves [69,70]. Some other studies that account for
 125 merger effects via the use of complete numerical simu-
 126 lations [45] are limited in the binary parameter space
 127 they sample. Others that do the same through the use of
 128 phenomenological waveform models [65,71] use the Fisher
 129 matrix to estimate Λ_{NS} measurement errors. Fisher matrix
 130 estimates may become unreliable at realistic signal-to-noise
 131 ratios (SNRs) [72], such as those as we might expect in the
 132 upcoming observing runs of GW detectors [31], and we
 133 improve such studies with a fully Bayesian treatment of the
 134 problem here.

135 In this paper we study the measurability of neutron star’s
 136 tidal deformability from realistic binaries of *low-mass* BHs
 137 and NSs by aLIGO. We also probe how tidal effects affect
 138 the estimation of other binary parameters for the same class
 139 of systems. This study improves upon previous work in the
 140 following ways. First, we include tidal effects during
 141 inspiral and merger in a consistent way, by using the
 142 waveform model of Lackey *et al.* [65] (abbreviated
 143 henceforth to “LEA”). Second, we include the effect of
 144 black hole spin on tidal GW signals, in addition to the effect
 145 of BH mass, tidal deformability of the NS, and the SNR.
 146 Third, we perform a complete Bayesian analysis, instead of
 147 using the Fisher matrix approximation. Fourth, we explore
 148 how our measurement errors decrease as we gain informa-
 149 tion from multiple (realistic) events.

150 We now outline the main questions and results discussed
 151 in this paper. First, we probe the effect of ignoring tidal
 152 effects in the recovery of nontidal binary parameters, such
 153 as component masses and spins. This is the case for current
 154 and planned aLIGO efforts. To do so, we first use the
 155 enhanced-LEA (or “LEA+,” see Sec. II A) model to
 156 generate a set of realistic signals; and then use nontidal
 157 (BBH) waveform filters to estimate the underlying binary
 158 masses and spins with a Markov-chain Monte Carlo. Here
 159 and throughout, we use the zero-detuning high-power
 160 design sensitivity curve [1] to characterize the expected
 161 detector noise. We find that, for individual events, ignoring
 162 tidal effects will affect mass and spin estimation only
 163 marginally; only for very loud signals (SNRs $\gtrsim 30$) will the
 164 systematic biases be large enough to exceed the underlying
 165 statistical uncertainty. Furthermore, detection searches can
 166 ignore tidal effects without loss of sensitivity.

167 Second, we study the ability of aLIGO to constrain
 168 neutron star tidal deformability with a single observation of
 169 an NSBH merger. For this, we use the same setup for signal
 170 waveforms as before, but replace the filter template model
 171 with one that includes tidal effects from inspiral through to
 172 merger (i.e. LEA+) [65]. For most binaries with BH
 173 masses outside of the mass gap ($2-5 M_{\odot}$ [73–76] and/or
 174 realistic signal-to-noise ratios (SNR), we find it difficult to

¹The upper limit on BH mass that allows for NS disruption may very well be higher, depending strongly on the magnitude of BH spin [46].

put better than a factor of 2 bound on Λ_{NS} with a single observation. As we can see from Fig. 6, it is only at SNRs $\rho \gtrsim 20$ –30 (under otherwise favorable circumstances, such as a stiff equation of state) that we are able to bring this down to a $\pm 75\%$ bound on Λ_{NS} . For signals louder than $\rho = 30$, we can constrain Λ_{NS} to a much more meaningful degree (within $\pm 50\%$ of its true value). While this is discouraging at first, we turn to ask: what if we combine information from a population of low-SNR observations?

The EoS of matter at nuclear densities is believed to be universal among all neutron stars. The Tolman–Oppenheimer–Volkoff equation [77–79] would then predict that NS properties satisfy a universal relationship between Λ_{NS} and m_{NS} . As the final part of this paper, we combine information from multiple observations of realistic NSBH systems and perform a fully Bayesian analysis of how our estimation of Λ_{NS} changes as we accumulate detections. This is similar to an earlier study [80] aimed at binary neutron stars. We restrict ourselves to a population of NSs with masses clustered very tightly around $1.35 M_{\odot}$ (with a negligible variance), and negligible spins. We sample different nuclear EoSs by sampling entire populations fixing different values for the NS tidal deformability. For all populations, we take source locations to be uniformly distributed in spatial volume, and source orientations to be uniform on the 2-sphere. To summarize, we find the following: (a) Our median estimate for Λ_{NS} starts out prior dominated, but converges to within 10% of the true value within 10–20 detections. (b) Measurement uncertainties for Λ_{NS} , on the other hand, depend on Λ_{NS} itself. We find that for hard equations of state (with $\Lambda_{\text{NS}} \geq 1000$), 10–20 observations are sufficient to constrain Λ_{NS} within $\pm 50\%$. For softer equations of state, the same level of certainty would require substantially more (25–40) observations. (c) Further, if the astrophysical “mass gap” [73–76] is real, we find that 20%–50% additional observations would be required to attain the same measurement accuracy as above. (d) Putting tighter constraints on the Λ_{NS} of a population would require 50+ NSBH observations, in any scenario. (e) It is the loudest 5–10 events that will furnish the bulk of tidal information, and not the combination of a large number of low-SNR events. All of the above is possible within a few years of design aLIGO operation [81].

In this paper, we restrict our parameter space to span mass ratios $q := m_{\text{BH}}/m_{\text{NS}} \in [2, 5]$, dimensionless BH spin (aligned with orbit) $\chi_{\text{BH}} \in [-0.5, +0.75]$, and dimensionless NS tidal deformability $\Lambda_{\text{NS}} := G(\frac{c^2}{Gm_{\text{NS}}})^5 \lambda \in [500, 2000]$. These ranges are governed by the calibration of the LEA+ model which we use as filters. Most of the disruptive NSBH simulations that LEA+ has been calibrated to involve $1.35 M_{\odot}$ NSs, and it is unclear how reliable the model is for different NS masses [65,82]. This motivates us to conservatively fix NS masses to $1.35 M_{\odot}$ in our simulated signals (not templates). But, since the domain

of calibration of LEA+ excludes NS spin completely, we fix $\chi_{\text{NS}} = 0$ in both signals as well as filter templates. We expect the effect of ignoring NS mass and spin variations in our NSBH populations to be less severe than for BNSs [83], considering the higher mass ratios of NSBHs. The accuracy of our quantitative results depends on the reliability of LEA+, which is the only model of its kind in current literature. A more recent work [82] improves upon the amplitude description of LEA+, but needs to be augmented with a compatible phase model. Overall, we expect our broad conclusions here to hold despite modeling inaccuracies (with errors not exceeding $\mathcal{O}(10\%)$ [82]). Finally, our results apply to LIGO instruments at design sensitivity, which they are projected to attain by 2019 [1,50].

The remainder of the paper is organized as follows. Section II discusses data analysis techniques and resources used in this paper, such as the waveform model, and parameter estimation algorithm. Section III discusses the consequences of ignoring tidal effects in parameter estimation waveform models. Section IV discusses the measurability for the leading order tidal parameter Λ_{NS} at plausible SNR values. Section V discusses the improvement in our measurement of Λ_{NS} with successive (multiple) observations of NSBH mergers. Finally, in Sec. VI we summarize our results and discuss future prospects with Advanced LIGO.

II. TECHNIQUES

A. Waveform models

Lackey *et al.* (LEA) [65] developed a complete inspiral-merger waveform model for disrupting NSBHs. Theirs is a frequency-domain phenomenological model that includes the effect of BH and NS masses and spins $\{m_{\text{BH}}, \chi_{\text{BH}}, m_{\text{NS}}\} \equiv \vec{\theta}$ and NS tidal deformability Λ_{NS} . It was calibrated to a suite of 134 numerical relativity (NR) simulations of NSs inspiraling into spinning BHs, with NS masses ranging between $1.2 M_{\odot} \leq m_{\text{NS}} \leq 1.45 M_{\odot}$, mass ratios $2 \leq q \leq 5$, and BH spins $-0.5 \leq \chi_{\text{BH}} \leq +0.75$. They also sample a total of 21 two-parameter nuclear EoSs to cover the spectrum of NS deformability. The GW strain $\tilde{h}(f)$ per the LEA model can be written as

$$\tilde{h}_{\text{NSBH}}(f, \vec{\theta}, \Lambda_{\text{NS}}) = \tilde{h}_{\text{BBH}}(f, \vec{\theta}) A(f, \vec{\theta}, \Lambda_{\text{NS}}) e^{i\Delta\Phi(f, \vec{\theta}, \Lambda_{\text{NS}})}, \quad (1)$$

with NS spin $\chi_{\text{NS}} = 0$ identically. Here, \tilde{h}_{BBH} is an underlying BBH waveform model. In the original LEA model, this was taken to be the SEOBNRv1 model [84] of the effective one body (EOB) family [85]. The factor $A(\cdot)$ adjusts the amplitude of the BBH model to match that of an NSBH merger of otherwise identical parameters, with NS-matter effects parametrized by Λ_{NS} . During early inspiral this term is set to unity, but is a sensitive function of Λ_{NS} .

close to merger. The term with $\Delta\Phi$ corrects the waveform phasing. During inspiral, $\Delta\Phi$ is set to the PN tidal phasing corrections, at the leading and next-to-leading orders [67]; close to merger, additional phenomenological terms are needed. Both A and $\Delta\Phi$ are calibrated to all 134 available NR simulations.

In this paper we use LEA for our signal and template modeling, but switch the underlying BBH model to SEOBNRv2 (and refer to it as enhanced-LEA or “LEA+”) [86]. We use the reduced-order frequency-domain version of SEOBNRv2, which has the additional benefit of reducing computational cost [87]. We expect this enhancement from LEA → LEA+ to make our conclusions more robust because: (a) the SEOBNRv2 model is more accurate [88,89], and (b) the differences between the two EOB models are caused by the inaccuracies of SEOBNRv1 during the *inspiral* phase, many orbits before merger [88]. Since LEA only augments inspiral phasing with PN tidal terms, our change in the underlying BBH model does not change LEA’s construction, *and* increases the overall model accuracy during inspiral. Finally, we note that we approximate the full GW signal with its dominant $l = |m| = 2$ modes, which are modeled by LEA+. For use in future LIGO science efforts, we have implemented the LEA+ model in the LIGO ALGORITHMS LIBRARY [90].

B. Bayesian methods

The process of measuring systematic and statistical measurement errors involves simulating many artificial GW signals, and inferring source binary parameters from them using Bayesian statistics. We start with generating a signal waveform, using the model LEA+, and injecting it in zero noise to obtain a stretch of data d_n . Source intrinsic parameters $\vec{\Theta} := \{m_{\text{BH}}, m_{\text{NS}}, \chi_{\text{BH}}, \Lambda_{\text{NS}}\}$ are reconstructed from this injected signal. Extrinsic parameters $\vec{\theta} := \{t_c, \phi_c\}$ representing the time of and phase at the arrival of signal are marginalized over numerically and analytically (respectively), while source location and orientation parameters such as its luminosity distance, sky location, inclination and polarization angles are absorbed into a normalization, as described later, and subsequently maximized over. This is justified because in this paper we consider the *single-detector case*. Using Bayes’ theorem, the joint inferred probability distribution of $\vec{\Theta}$ can be evaluated as

$$p(\vec{\Theta}|d_n, H) = \frac{p(d_n|\vec{\Theta}, H)p(\vec{\Theta}|H)}{p(d_n|H)}. \quad (2)$$

Here, $p(\vec{\Theta}|H)$ is the *a priori* probability of binary parameters $\vec{\Theta}$ taking particular values, given H —which denotes all our collective knowledge, except for expectations on binary parameters that enter our calculations explicitly. Throughout this paper, we impose priors that are uniform in

individual component masses, BH spin, and the tidal deformability of the NS. In addition, we restrict mass ratios to $q \geq 2$, as LEA+ is not calibrated for $1 \leq q \leq 2$. $p(d_n|\vec{\Theta}, H)$ is the *likelihood* of obtaining the given stretch of data d_n if we assume that a signal parametrized by $\vec{\Theta}$ is buried in it, and is given by

$$p(d_n|\vec{\Theta}, H) \equiv \mathcal{L}(\vec{\Theta}) = \mathcal{N} \exp\left[-\frac{1}{2}\langle d_n - h|d_n - h\rangle\right], \quad (3)$$

where $h \equiv h(\vec{\Theta})$ is a filter template with parameters $\vec{\Theta}$, $\langle \cdot | \cdot \rangle$ is a suitably defined detector-noise weighted inner product,² and \mathcal{N} is the normalization constant that absorbs source distance, orientation and sky location parameters. As in Ref. [91] we use a likelihood that is maximized over the template norm, allowing us to ignore the extrinsic parameters that only enter in the template norm through \mathcal{N} . As a result, we only need to sample over $\vec{\Theta}$ (or $\vec{\Theta} - \{\Lambda_{\text{NS}}\}$ in the case of nontidal templates). The denominator in Eq. (2) is the *a priori* probability of finding the particular signal in d_n and we assume that each injected signal is as likely as any other. From the joint probability distribution $p(\vec{\Theta}|d_n, H)$ so constructed, extracting the measured probability distribution for a single parameter (say α) involves integrating

$$p(\alpha|d_n, H) = \int d\vec{\Theta}_\alpha p(\vec{\Theta}|d_n, H), \quad (5)$$

where $\vec{\Theta}_\alpha$ is the set of remaining parameters, i.e. $\vec{\Theta}_\alpha := \vec{\Theta} - \{\alpha\}$.

We use the ensemble sampler Markov-chain Monte Carlo algorithm implemented in the EMCEE package [92], to sample the probability distribution $p(\vec{\Theta}|d_n, H)$. We run 100 independent chains, each of which is allowed to collect 100,000 samples and combine samples from chains that have a Gelman-Rubin statistic [93] close to unity. This procedure yields about 10,000 independent samples. One simplification we make to mitigate computational cost is to set the frequency sampling interval to $\Delta f = 0.4$ Hz, which we find to be sufficient for robust likelihood calculations in zero noise [91]. We integrate Eq. (5) to obtain marginalized probability distributions for the NS tidal deformability

²The inner product $\langle \cdot | \cdot \rangle$ is defined as

$$\langle a|b \rangle \equiv 4\text{Re} \left[\int_0^\infty \frac{\tilde{a}(f)\tilde{b}(f)^*}{S_n(|f|)} df \right], \quad (4)$$

where $\tilde{a}(f)$ is the Fourier transform of the finite time series $a(t)$, and $S_n(|f|)$ is the one-sided amplitude spectrum of detector noise. In this work, we use the zero-detuning high-power design sensitivity curve [1] for Advanced LIGO, with 15 Hz as the lower frequency cutoff.

parameter: $p(\Lambda_{\text{NS}}|d_n, H)$. We will quote the median value of this distribution as our *measured* value for Λ_{NS} , and the 90% credible intervals associated with the distribution as the statistical error bars.

III. HOW IS PE AFFECTED IF WE IGNORE NS MATTER EFFECTS?

Past (and future) efforts with Advanced LIGO have used (or plan to use) BBH waveform templates to search for and characterize NSBH sources. In doing so, they ignore the signature of NS tidal effects on the emitted GWs. In this section we present a fully Bayesian analysis of the effect of this simplification on the recovery of nontidal parameters from NSBH signals.

We inject LEA + NSBH signals into zero noise, and run a Markov-chain Monte Carlo sampler on them using equivalent BBH templates (same model, tidal terms $\rightarrow 0$). We fix $m_{\text{NS}} = 1.35 M_{\odot}$ and $\chi_{\text{NS}} = 0$, and explore a range of NS equations of state via the single tidal deformability parameter $\Lambda_{\text{NS}} \in \{500, 800, 1000, 1500, 2000\}$. Our injections also span a rectangular grid in the BH parameter space, with vertices at $q \in \{2, 3, 4, 5\}$, i.e. $m_{\text{BH}} \in \{2.7 M_{\odot}, 4.05 M_{\odot}, 5.4 M_{\odot}, 6.75 M_{\odot}\}$, and BH spins $\chi_{\text{BH}} \in \{-0.5, 0, +0.5, +0.75\}$. Finally, we sample all other source-related parameters that determine the signal strength but not character,³ by sampling the SNR $\rho \in \{20, 30, 50, 70\}$. Our choice of injection parameters here is motivated by two factors: (i) previous studies of the signatures of NS tidal effects on gravitational waves [45,46,95] (which suggest that necessary conditions for the observation of tidal effects with aLIGO include high SNRs and a low-mass spinning companion BH); and (ii) technical constraints of our chosen LEA+model [65]. At design sensitivity, if we expect 0.2–300 NSBH detections a year [81], we can expect to see 0.02–25 *disruptive*⁴ NSBH mergers a year, of which we will have 0.005–7 observations with $\rho \geq 20$, and 0.002–3 a year with $\rho \geq 30$. Therefore, our injection parameters span a physically interesting subset of NSBH binaries, which is *also* likely observable in the near future. For our Bayesian priors, we choose uniform distributions for both component masses and black hole spin: $m_{\text{BH}} \in [1.2, 25]M_{\odot}$; $m_{\text{NS}} \in [1.2, 3]M_{\odot}$; and $-0.75 \leq \chi_{\text{BH}} \leq +0.75$.

³For aligned-spin signals and aligned-spin templates both, we only consider the contribution of the dominant $l = |m| = 2$ waveform multipoles. This approximation has the additional benefit of combining the dependence of the waveforms on inclination, polarization and sky location angles, as well as on distance, into the luminosity or *effective* distance. This quantity only appears as an overall scaling factor, and therefore only affects signal strength [94].

⁴We assume here that BH mass values are *uniformly* likely from $2 M_{\odot}$ to $\sim 35 M_{\odot}$ [2], but NSs are disrupted in NSBH mergers only if $q \leq 6$ and $\chi_{\text{BH}} \geq 0$ [45,46].

The effect of ignoring tidal corrections in templates will manifest as a systematic shift of recovered median parameter values away from what they would be if we had used tidal templates with identical priors. In zero noise, we expect the probability distributions recovered using tidal templates to be multidimensional Gaussians with the maximum likelihood parameter values approaching their true values. If the priors are not restrictive, we expect the recovered median to also converge to the true value. However, the LEA model imposes significantly more restrictive priors (both mass ratio and spin) than SEOBNRv2 [65,86], which shifts the median value of parameters recovered using *our* tidal templates away from their true value. If we use LEA+ priors for our nontidal templates, it would add a caveat to our original question “can we estimate nontidal NSBH parameters with equivalent BBH templates.” Instead, we approximate the median tidally recovered parameters by their true injected values, as one would expect to recover with an ideal model for tidally disruptive NSBH mergers. With this caveat, we estimate *systematic* measurement bias/errors as the differences between median and *injected* parameter values. As an illustration, in Fig. 1 we show the recovered probability distributions for binary mass ratio η for three NSBH injections, with $\rho = 20$ (left), 30 (middle), and $\rho = 50$ (right), and other parameters held fixed ($m_{\text{NS}} = 1.35 M_{\odot}$, $\chi_{\text{NS}} = 0$, $m_{\text{BH}} = 5.4 M_{\odot}$, $\chi_{\text{BH}} = +0.5$ and $\Lambda_{\text{NS}} = 2000$). In each panel, both the *true* and median values of η are marked, and we use the shift between the red and green vertical lines as our estimate of systematic measurement errors. Darker shading in all panels marks 90% credible intervals, whose width $(\Delta\eta)^{90.0\%}$ we use as a direct measure of our *statistical* measurement uncertainty/error.⁵ For the illustrated binary, we see clearly that even when the signal is moderately loud, with $\rho = 20$, statistical errors dominate over systematics for η . As we turn up the SNR further, the two error sources become comparable at $\rho \sim 30$, and systematic errors dominate finally when $\rho \simeq 50$.

Credible intervals $(\Delta X)^{90\%}$ showing the precision with which $X = \{\mathcal{M}_c, \eta, \chi_{\text{BH}}\}$ can be measured are presented in Appendix A. We remind ourselves that this *precision* is only meaningful so long as the measurement is *accurate* to begin with. Therefore, we define R_X as the ratio between systematic and statistical errors associated with the measurement of parameter X ,

$$R_X = \frac{(X^{\text{Median}} - X^{\text{Injected}})}{(\Delta X)^{90\%}}, \quad (6)$$

in order to compare the relative magnitude of both. Only when $|R_X| \ll 1$ can we ignore tidal effects in our templates

⁵We generalize the notation $(\Delta X)^{90.0\%}$ to mean the 90% credible interval width for any measured source parameter X .

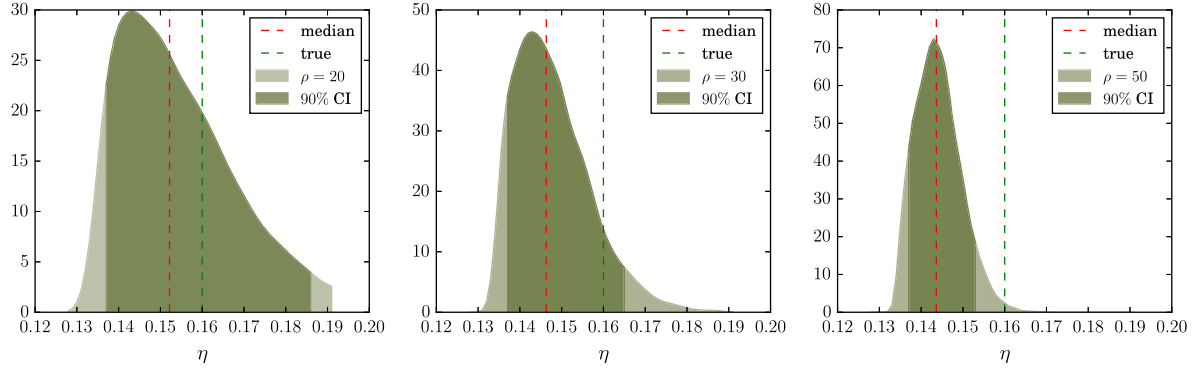


FIG. 1. Illustrative posterior probability distributions for mass ratio η at different SNR values: We show here probability distributions for mass ratio η as measured for the same signal at different SNRs. The intrinsic parameters of the source are: $q = m_{\text{BH}}/m_{\text{NS}} = 5.4 M_{\odot}/1.35 M_{\odot} = 4$, $\chi_{\text{BH}} = +0.5$, and $\Lambda_{\text{NS}} = 2000$; and the signal is injected at SNRs $\rho = \{20, 30, 50\}$ (left to right). The templates ignore tidal effects. In each panel, the dashed red line marks the median value η^{Median} , while the dashed green line shows the true value η^{Injected} . The darker shading shows the recovered 90% credible interval for η , $(\Delta\eta)^{90\%}$. Comparing systematic and statistical errors, we find that, at $\rho = 20$, the η measurement is dominated by statistical errors; at $\rho = 30$, the two become comparable; and for louder signals ($\rho \simeq 50$), the systematic errors dominate.

without hampering the measurement of nontidal parameters from NSBH signals. When R_X approaches a few tens of percent of unity, we can begin to favor tidal templates for NSBH studies.

We start with calculating $R_{\mathcal{M}_c}$ as a function of various source parameters and show it in Fig. 2. \mathcal{M}_c is the leading order mass combination that affects the GW strain emitted by compact binaries as they spiral in, and is therefore

determined the most precisely. We notice immediately that for $\rho \leq 30$ the systematics are well under control and we can obtain reliable chirp mass estimates for NSBH signals using BBH templates. For louder and less likely SNRs ($\rho \simeq 50$), we find that $R_{\mathcal{M}_c}$ can become comparable to unity, but only if the BH has prograde spin $\chi_{\text{BH}} \gtrsim 0.4$, and the true NS tidal deformability is large enough, such that $\Lambda_{\text{NS}} \gtrsim 1000$. We therefore conclude that only for very loud

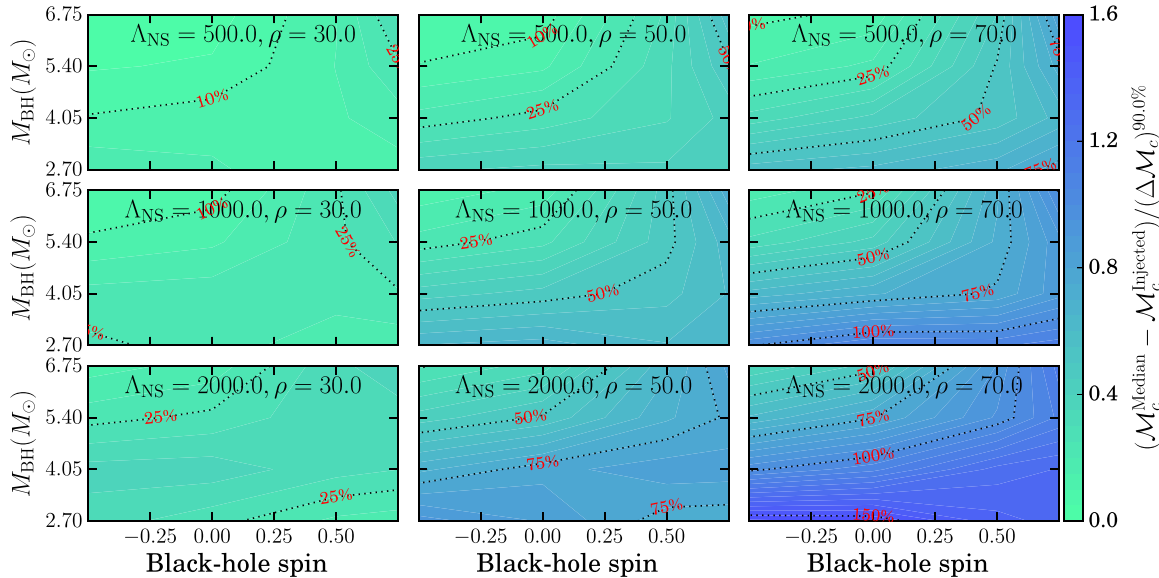


FIG. 2. Ratio of systematic to statistical errors in measuring \mathcal{M}_c , ignoring tidal effects: We show here the ratio of systematic and statistical measurement uncertainties for the binary chirp mass over the NSBH parameter space. Each panel shows the same as a function of BH mass and spin. NS mass is fixed at $m_{\text{NS}} = 1.35 M_{\odot}$, and its spin is set to zero. Down each column, we can see the effect of the increasing tidal deformability of the NS at fixed SNR. Across each row, we can see the effect of increasing the signal strength (SNR), with the tidal deformability of the NS fixed. We show dashed contours for $R_{\mathcal{M}_c} = 10\%, 25\%, 50\%, \dots$, with interleaving filled color levels separated by 5%. For BBHs, the statistical errors dominate systematic ones for contemporary waveform models [89,97]. We find that it is not much different for NSBH binaries, until we get to very high SNRs $\rho \gtrsim 70$.

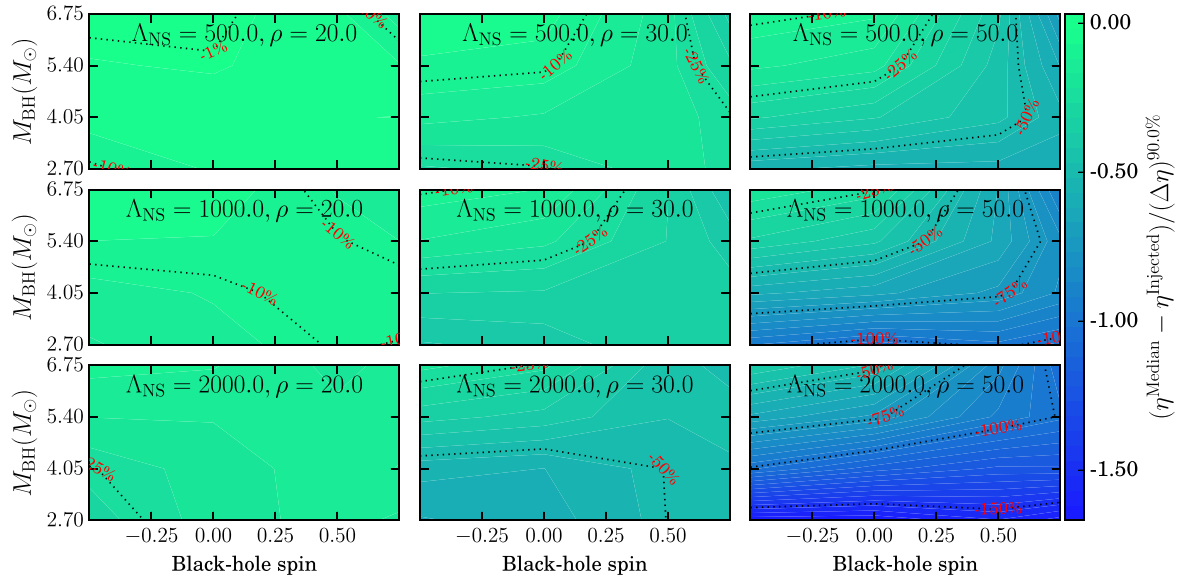


FIG. 3. Ratio of systematic to statistical errors in measuring η , ignoring tidal effects: This figure is similar to Fig. 2 with the difference that here we show the ratio of systematic and statistical error sources for the symmetric mass ratio η and not chirp mass. We find that for fairly loud GW signals, at $\rho \approx 50$, not including the effects of tidal deformation of the NS on GW emission can become the dominant source of error for astrophysical searches with Advanced LIGO. However, for quieter signals with $\rho \leq 30$, it will have a negligible effect on the measurement of η . We remind the reader that the SNRs here are always single detector values.

signals, with $\rho \gtrsim 50\text{--}70$, will the inclusion of tidal terms in template models improve \mathcal{M}_c estimation. For lower SNRs, inclusion of new physical content in templates will instead get washed out by detector noise. In addition, we also note that $R_{\mathcal{M}_c} \geq 0$ always, i.e. \mathcal{M}_c is always being overestimated. This is to be expected since the tidal deformation of the NS drains energy faster from the orbit during inspiral (as compared to the BBH case), and its disruption close to merger reduces GW signal power at high frequencies. Both of these effects make the resulting signal resemble a BBH signal of higher chirp (or total) mass, although we expect the latter effect to be dominant [96].

Next, in Fig. 3, we show the ratio of measurement errors R_η for the symmetric mass-ratio. Going through the figure from left to right, we find that for realistic SNRs ($\rho \leq 30$) the systematics remain below statistical errors for η measurement. The worst case is of the most deformable NSs ($\Lambda_{\text{NS}} = 2000$), but even for them systematics in η are $2\times$ smaller than the statistical measurement errors. Moving to louder signals with $\rho \approx 50$, we find that for binaries of fairly deformable NSs ($\Lambda_{\text{NS}} \gtrsim 1500$) and low-mass BHs ($m_{\text{BH}} \leq 5 M_\odot$) that have prograde spins ($\chi_{\text{BH}} \gtrsim +0.4$), our measurement of mass ratio can be seriously compromised by ignoring tidal physics in template models. This pattern is continued at even higher SNRs, as we can see from Fig. 3. We therefore conclude that, even if under moderate restrictions on BH and NS parameters, $\rho = 30\text{--}50$ is loud enough to motivate the use of tidal templates in aLIGO data analyses. In addition, we also notice that, unlike for \mathcal{M}_c , the median value of η is always *lower* than its true value,

which is what we expect if we want BBH templates to fit NSBHs that disrupt and merge at lower frequencies.

Moving on from mass to spin parameters, we now consider the measurement of BH spin angular momentum χ_{BH} . The ratio of systematic and statistical errors for χ_{BH} are shown in Fig. 4. The presentation of information in this figure is identical to that of Figs. 2 and 3. A diverging color map is used so that both extremes of the color bar range point to large systematic biases, while its zero (or small) value lies in the middle. For the lowest SNR considered ($\rho = 30$), χ_{BH} bias is about $2\times$ smaller than its statistical measurement uncertainty, and is therefore mostly negligible. Both do become somewhat comparable, but only when we have the most deformable NSs in orbit around low-mass BHs. At higher SNRs ($\rho \approx 50\text{--}70$), we find that the systematics in χ_{BH} measurement can dominate completely, especially for binaries containing mass-gap violating BHs and/or deformable NSs with $\Lambda_{\text{NS}} \geq 1000$. From Fig. 4 we additionally note that when the source spin magnitudes approach the highest allowed, i.e. at both extremes of the x axes, $\chi_{\text{BH}} \times R_{\chi_{\text{BH}}} < 0$. This is to be expected because the median of the recovered posterior distributions for χ_{BH} can only get pushed inwards from the boundaries.

Summarizing these results, we find that irrespective of system parameters, below a signal-to-noise ratio of 30, our measurements of mass and spin parameters of astrophysical NSBH binaries will remain limited by the intrinsic uncertainty due to instrument noise, and do not depend on whether we include tidal effects in template models.

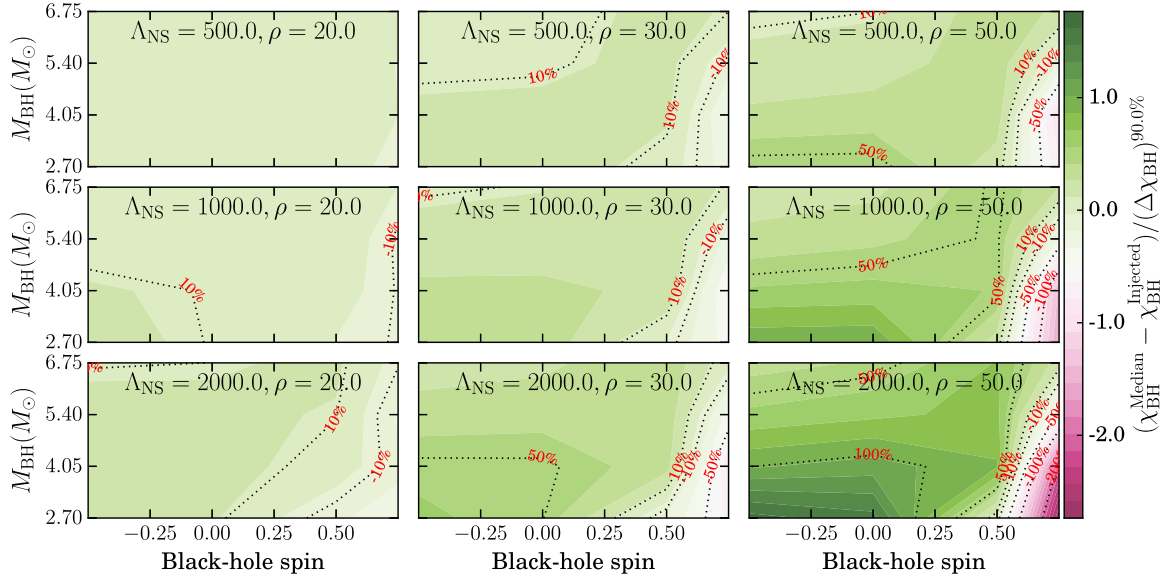


FIG. 4. Ratio of systematic to statistical errors in measuring χ_{BH} , ignoring tidal effects: This figure shows the ratio of the systematic and statistical measurement errors for BH spins $R_{\chi_{\text{BH}}}$. Information is arranged identically to Figs. 2, and 3, with the level spacing of filled contours increased to 15%. Similar to the case of mass parameters, we find that below $\rho \approx 30$, ignoring tidal effects in templates introduces minor systematic effects, which remain subdominant to the statistical measurement uncertainties.

However, when the signal-to-noise ratio exceeds 30 the systematic bias in binary mass and spin measurements become comparable to and can exceed the uncertainty due to noise. Of the different nontidal parameters considered, we find that the measurement of η degrades worst (in a relative-error sense) due to the use of BBH templates in deciphering an NSBH signal. Of all the subcategories, we find that tidal templates could especially help with the parameter estimation of astrophysical *mass-gap violating* NSBH binaries.

IV. WHAT DO WE GAIN BY USING TEMPLATES THAT INCLUDE NS MATTER EFFECTS?

In the previous section, we showed that the effects of the tidal deformation of NSs by their companion BHs become discernible in the GW spectrum under certain favorable conditions, including (a) BH mass is sufficiently small, (b) BH spin is positive aligned, i.e. $\chi_{\text{BH}} \gtrsim +0.4$, (c) the NS is not very compact, with $\Lambda_{\text{NS}} \gtrsim 1000$, and (d) the source location and orientation are such that its GW SNR $\gtrsim 30$. Both conditions (a) and (b) enhance the tidal distortion of the star and increase the number of orbits the system goes through at small separation, where the differences between NSBH and BBH signals are maximal. Conditions (a)–(c) also reduce the onset frequency of the disruption of the NS, allowing for it to happen earlier in the orbit. We expect that these conditions are also the ones which should maximize the likelihood of *measuring* tidal effects in NSBH signals. Here, we turn the question around to ask: under similarly favorable circumstances, can we gain insights about the internal structure of neutron stars from GW observations?

In this section, we calculate the accuracy with which we measure Λ_{NS} from *single* GW observations. We sample the same set of disruptive NSBH mergers as in the previous section, i.e. those with $q = \{2, 3, 4, 5\}$, $\chi_{\text{BH}} = \{-0.5, 0, +0.5, +0.75\}$, and $\Lambda_{\text{NS}} = \{500, 800, 1000, 1500, 2000\}$; fixing the NS mass $m_{\text{NS}} = 1.35 M_{\odot}$ and $\chi_{\text{NS}} = 0$. For each unique combination of these parameters, we inject LEA+ signals into zero noise and perform a fully Bayesian parameter estimation analysis of each with LEA+ templates. Our priors on component masses and spins remain as in the previous section, with mass ratio additionally restricted to $2 \leq q \leq 6$, and Λ_{NS} sampled uniformly from $[0, 4000]$. As an illustration of individual injections, we show the recovered probability distribution for Λ_{NS} for three specific configurations in Fig. 5. We fix $q = m_{\text{BH}}/m_{\text{NS}} = 5.4 M_{\odot}/1.35 M_{\odot} = 4$, with $\chi_{\text{BH}} = +0.5$, and vary Λ_{NS} over $\{1000, 1500, 2000\}$ between the three panels. The SNR is fixed at $\rho = 50$. The darker shaded regions mark the 90% credible interval on Λ_{NS} . We note that Λ_{NS} is estimated to within ± 2000 of its true value at this SNR. Another interesting thing to note is that while $(\Delta\Lambda_{\text{NS}})^{90\%}$ slowly grows with Λ_{NS} , the fractional uncertainty

$$\delta\Lambda_{\text{NS}}^{90\%} := (\Delta\Lambda_{\text{NS}})^{90\%}/\Lambda_{\text{NS}} \quad (7)$$

decreases instead. Further illustrations, showing the correlation between tidal and nontidal parameters, are presented in Appendix B. We will continue here to focus on the measurement of Λ_{NS} itself.

In Fig. 6 we show the main results of this section. In each panel, as a function of black hole mass and spin, we show

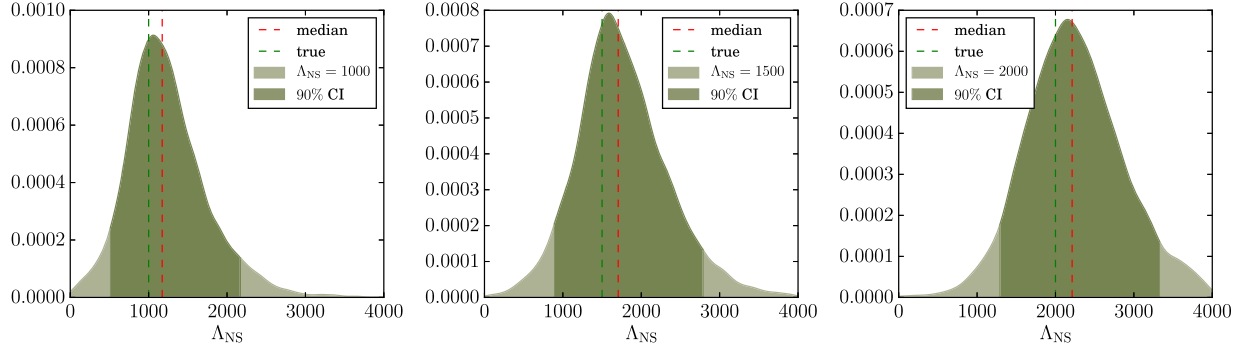


FIG. 5. Illustrative posterior probability distributions for NS tidal deformability Λ_{NS} : We show here probability distributions recovered for the NS tidal deformability parameter Λ_{NS} from three GW injections, with parameters $q = m_{\text{BH}}/m_{\text{NS}} = 5.4 M_{\odot}/1.35 M_{\odot} = 4$, $\chi_{\text{BH}} = +0.5$, and $\Lambda_{\text{NS}} = \{1000, 1500, 2000\}$ from left to right. The injection SNR is fixed at $\rho = 50$. The templates include tidal effects, with a prior $0 \leq \Lambda_{\text{NS}} \leq 4000$. In each panel, the dashed red line marks the median value for Λ_{NS} , and the dashed green line marks its *true* value. The darker shading shows the 90% credible interval, whose width $(\Delta\Lambda_{\text{NS}})^{90\%}$ is a direct measure of our statistical uncertainty. By comparing the measurement uncertainty for these three injections, we see that $(\Delta\Lambda_{\text{NS}})^{90\%}$ grows very slowly with Λ_{NS} . Therefore, the fractional measurement error— $(\Delta\Lambda_{\text{NS}})^{90\%}/\Lambda_{\text{NS}}$ —decreases monotonically as Λ_{NS} increases (with signal strength fixed).

the measured 90% credible interval widths $(\Delta\Lambda_{\text{NS}})^{90\%}$. These correspond to the full width of the dark shaded regions in the illustrative Fig. 5. The effect of increasing signal strength can be seen as we go from left to right in each row. The effect of the NS tidal deformability parameter Λ_{NS} on its own measurability can be seen by

comparing panels within each column, with the NS becoming more deformable from top to bottom. A uniform pattern emerges in the leftmost column, which corresponds to $\rho = 20$. We find that at this signal strength, our measurement of Λ_{NS} is dominated by the width of our prior on it. The 90% credible intervals span the entire

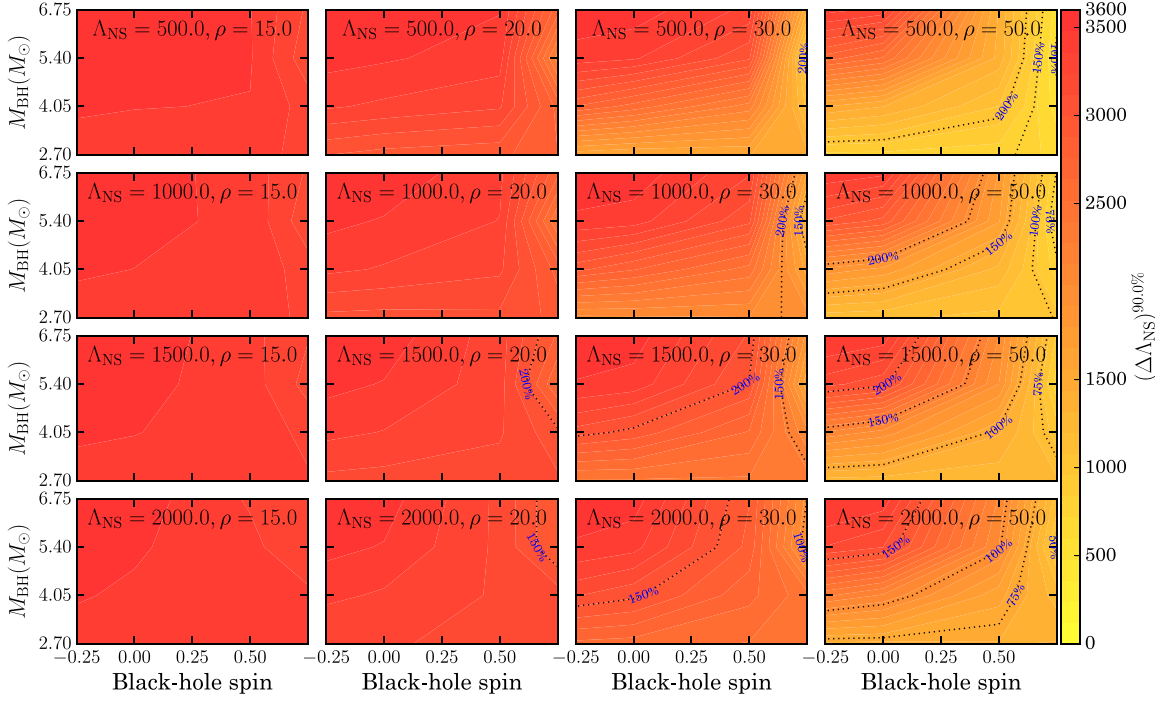


FIG. 6. Statistical uncertainty in Λ_{NS} measurement: Here we show the statistical uncertainty in the measurement of Λ_{NS} . In each panel, the same is shown as a function of the BH mass and spin, keeping Λ_{NS} and injection's SNR ρ fixed (noted in the panel). Rows contain panels with the same value of Λ_{NS} , with ρ increasing from left to right. Columns contain panels with the same value of ρ , with Λ_{NS} increasing from top to bottom. Contours at $(\Delta\Lambda_{\text{NS}})^{90\%} = \{50\%, 75\%, 100\%, 150\%, 200\%\} \times \Lambda_{\text{NS}}^{\text{Injected}}$ demarcate regions where we can constrain the Λ_{NS} parameter well (within a factor of 2 of the injected value). We note that, as expected, the measurement accuracy for Λ_{NS} improves with (i) increasing SNR, (ii) increasing Λ_{NS} , (iii) increasing BH spin, and (iv) decreasing BH mass.

allowed range for Λ_{NS} , making a reasonable estimation of Λ_{NS} at $\rho \approx 20$ difficult. Increasing the signal strength to $\rho = 30$ gives marginally better results, bringing down the statistical uncertainties to within $\pm 75\text{--}100\%$ of the true Λ_{NS} value.⁶ It is not until we reach an SNR as high as $\rho \gtrsim 50$, can we put meaningful [i.e. $\mathcal{O}(10\%)$] constraints on Λ_{NS} . For example, with a *single* observation of a $q = 4$ binary with $\chi_{\text{BH}} \geq 0.6$ and $\rho = 50$,⁷ we would be able to estimate Λ_{NS} to within $\pm 40\%$ of its true value (which is equivalent to measuring the ratio of NS radius to mass with an uncertainty of about $\pm 10\%$). These results agree well with Sec. III, and are consistent with Fisher matrix estimates at high SNRs [65].

Amongst other source parameters, BH mass and spin play a dominant role. A smaller BH with a larger spin always allows for a more precise measurement on Λ_{NS} . We can see this in the bottom right corner of each panel in Fig. 6, which corresponds to low-mass BHs with large spins, and is simultaneously the region of smallest measurement errors on Λ_{NS} . The actual deformability of the NS also plays an important role on its own measurability. For example, when $\Lambda_{\text{NS}} \leq 1000$, it is fairly difficult to meaningfully constrain Λ_{NS} without requiring the source to be close (≈ 100 Mpc) with a GW SNR $\rho \gtrsim 50$. Quantifying this further, in Fig. 7 we show the minimum signal strength required to attain a certain level of credibility in our Λ_{NS} measurement, as a function of BH properties. The NS is allowed the most favorable (hardest) EoS considered, with $\Lambda_{\text{NS}}^{\text{true}} = 2000$. We first note that, even with the most favorable BH and NS properties, achieving a $\pm 50\%$ measurement certainty on Λ_{NS} will require a GW SNR $\rho \gtrsim 30$. If we additionally restrict BH masses to lie outside of the so-called astrophysical mass gap [73–76], we will simultaneously need to restrict BH spins to $\chi_{\text{BH}} \gtrsim +0.5$ to obtain the same measurement credibility at the same source location.

It is interesting to note that the parameter ranges most favorable to the measurability of Λ_{NS} are also those which produce relatively more massive postmerger disks [44]. That is, the subset of NSBHs that potentially produce SGRBs (using a sufficiently large disk mass as an indicator) would be the same subset most favorable for measurement of tidal effects. Therefore the rate of SGRBs in the local universe (allowing for the fraction that are produced by NSBHs versus BNSs) would be an indicator of the rate of events most favorable for nuclear equation of state measurements.

In summary, with a single moderately loud ($\rho \lesssim 30$) GW signal from a disruptive BHNS coalescence, we can

⁶The symmetric error bars of $\pm X\%$ correspond to $\delta\Lambda_{\text{NS}}^{90\%} = 2X\%$.

⁷For an optimally oriented source with $q=4, m_{\text{NS}}=1.35 M_{\odot}, \chi_{\text{BH}}=0.6$, an SNR of $\rho = 50$ corresponds to a luminosity distance of ≈ 113 Mpc.

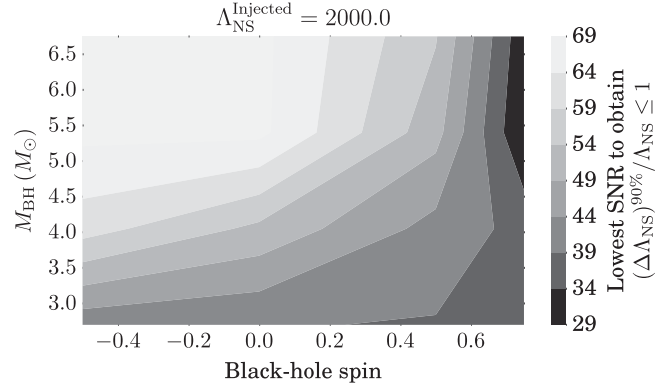


FIG. 7. We show here, as a function of BH mass and spin, the *minimum* signal strength (SNR) required to constrain Λ_{NS} within an interval of width equal to 100% of its true value, i.e. with $\pm 50\%$ error bars. The NS mass is fixed at $1.35 M_{\odot}$, spin at zero, and $\Lambda_{\text{NS}} = 2000$. We can see that, even in the most conducive circumstances with large aligned χ_{BH} and a comparable mass BH, we can only constrain Λ_{NS} to better than $\pm 50\%$ if the SNR is $\gtrsim 29$. In the era of design sensitivity LIGO instruments, we expect this to happen approximately once in a year of observation [81].

constrain the NS compactness parameter Λ_{NS} within $\pm 100\%$ of its true value. To measure better with one observation, we will need a more fine-tuned source, with $\rho \geq 30$ and high BH spins, or $\rho \geq 50$. Finally, we note that these results are *conservative*, and BHs with spins $\chi_{\text{BH}} > 0.75$ will prove to be even more favorable laboratories for Λ_{NS} measurement. However, we are presently unable to explore this case in quantitative detail due to waveform model restrictions [65], which will also restrict our analyses of GW signals during the upcoming LIGO observing runs.

V. COMBINING OBSERVATIONS: LOOKING FORWARD WITH ADVANCED LIGO

In the previous section, we showed that single observations of NSBH coalescences at moderate SNRs have little information about the internal structure of neutron stars that will be accessible to Advanced LIGO at its design sensitivity. We expect all neutron stars to share the same equation of state, and hence the same $\Lambda_{\text{NS}}(m_{\text{NS}})$. In addition, we know that the mass distribution of (most) NSs that have not been spun up to millisecond periods (which are the ones we focus on in this paper, by setting $\chi_{\text{NS}} \approx 0$) is narrowly peaked around $\sim 1.35 M_{\odot}$ [98]. Therefore, information from multiple NSBH observations can be combined to improve our estimation of Λ_{NS} . We explore the same in this section within a fully Bayesian framework. We refer the reader to Refs. [60,61,99] for similar analyses of BNS inspirals.

An intuitive understanding of the problem is gained by considering first multiple *identical* sources with realistic but different SNRs. Let us consider the case of a population

F7:1
F7:2
F7:3
F7:4
F7:5
F7:6
F7:7
F7:8
F7:9

647
648
649
650
651
652
653
654
655
656
657

658
659

660
661
662
663
664
665
666
667
668
669
670
671
672
673
674
675
676
677

of optimally oriented binaries,⁸ distributed uniformly in spatial volume out to a maximum *effective* distance⁹ D^{\max} . D^{\max} is set by the minimum SNR threshold ρ_{\min} at which a source is considered detectable.¹⁰ Next, we divide this volume into I concentric shells, with radii D_i . If we have a measurement error σ_0 for Λ_{NS} , associated with a source located at $D = D_0$, the same error for the same source located within the i th shell would be $\sigma_i = \sigma_0 \frac{D_i}{D_0}$. Reference [56] calculated that the combined error σ from N independent measurements of Λ_{NS} in such a setting to be

$$\begin{aligned} \frac{1}{\sigma^2} &= \sum_{i=1}^I \frac{N_i}{\sigma_i^2} = \left(\frac{D_0}{\sigma_0}\right)^2 \sum_{i=1}^I \frac{N_i}{D_i^2} \\ &= \left(\frac{D_0}{\sigma_0}\right)^2 \int_0^{D^{\max}} \frac{4\pi D^2 n}{D^2} dD = \left(\frac{D_0}{\sigma_0}\right)^2 \frac{3N}{(D^{\max})^2}, \end{aligned} \quad (8)$$

where N_i is the number of sources within the i th shell (such that $N := \sum N_i$), and n is the number density of sources in volume. The root-mean-square (rms) averaged measurement error from N sources is then [56]

$$\sigma_{\text{avg}} := \frac{1}{\sqrt{1/\sigma^2}} = \frac{\sigma_0}{D_0} D^{\max} \frac{1}{\sqrt{3N}}, \quad (9)$$

given a fiducial pair (σ_0, D_0) . It is straightforward to deduce from Eq. (9) that measurement uncertainty scales as $1/\sqrt{N}$, and the uncertainty afforded by a single observation with a high SNR ρ_c can be attained with $N = \rho_c^2/300$ realistic observations that have $\rho \geq \rho_{\min}$. E.g., to get to the level of certainty afforded by a single observation with $\rho = 70$, we would need $49/3 \approx 16$ –17 realistic (low SNR) detections.

While we discussed Eq. (9) for a population of optimally oriented sources, it is valid for a more general population distributed uniformly in effective volume [56] ($\propto D^3$). However, it still only applies to sources with identical masses and spins, and we overcome this limitation by performing a fully Bayesian analysis next.

A. Astrophysical source population

Imagine that we have N stretches of data, d_1, d_2, \dots, d_N , each containing a single signal emitted by an NSBH binary. Each of these signals can be characterized by the nontidal

⁸An optimally oriented binary is one which is located directly overhead the detector, with the orbital angular momentum parallel to the line joining the detector to the source. Such a configuration maximizes the observed GW signal strength in the detector.

⁹The *effective* distance D is a combination of distance to the source, its orientation, and its sky location angles; and has a one-to-one correspondence with SNR for nonprecessing sources. This is so because for such sources their location and orientation remain constant over the time scales within which they sweep through aLIGO's sensitive frequency band.

¹⁰We take this as $\rho_{\min} = 10$ throughout.

source parameters $\vec{\theta} := \{m_{\text{BH}}, m_{\text{NS}}, \chi_{\text{BH}}, \chi_{\text{NS}}, \vec{\alpha}\}$, and $\{\Lambda_{\text{NS}}\}$, where $\vec{\alpha}$ contains extrinsic parameters, such as source distance, inclination, and sky location angles. As before, let H denote all of our collective prior knowledge; for instance, H includes our assumption that all NSs in a single population have the same deformability parameter Λ_{NS} , and that its cumulative measurement is therefore possible. The probability distribution for Λ_{NS} , given N unique and independent events, is

$$\begin{aligned} p(\Lambda_{\text{NS}}|d_1, d_2, \dots, d_N, H) \\ = \frac{p(d_1, d_2, \dots, d_N|\Lambda_{\text{NS}}, H)p(\Lambda_{\text{NS}}|H)}{\int p(\Lambda_{\text{NS}}|H)p(d_1, d_2, \dots, d_N|\Lambda_{\text{NS}}, H)d\Lambda_{\text{NS}}}, \end{aligned} \quad (10)$$

$$= \frac{p(\Lambda_{\text{NS}}|H)\prod_i p(d_i|\Lambda_{\text{NS}}, H)}{\int p(\Lambda_{\text{NS}})p(d_1, d_2, \dots, d_N|\Lambda_{\text{NS}}, H)d\Lambda_{\text{NS}}}, \quad (11)$$

$$= \frac{p(\Lambda_{\text{NS}}|H)\prod_i (p(\Lambda_{\text{NS}}|d_i, H) \frac{p(d_i)}{p(\Lambda_{\text{NS}}|H)})}{\int p(\Lambda_{\text{NS}}|H)p(d_1, d_2, \dots, d_N|\Lambda_{\text{NS}}, H)d\Lambda_{\text{NS}}}; \quad (12)$$

where Eqs. (10) and (12) are application of Bayes' theorem, while Eq. (11) comes from the mutual independence of all events. Assuming in addition that all events are *equally likely*: $p(d_i) = p(d_j) = p(d)$, we get

$$\begin{aligned} p(\Lambda_{\text{NS}}|d_1, d_2, \dots, d_N, H) \\ = p(\Lambda_{\text{NS}})^{1-N} \times \frac{p(d)^N}{\int p(\Lambda_{\text{NS}})p(d_1, d_2, \dots, d_N|\Lambda_{\text{NS}}, H)d\Lambda_{\text{NS}}} \\ \times \prod_i p(\Lambda_{\text{NS}}|d_i, H), \end{aligned} \quad (13)$$

where the prior probability $p(\Lambda_{\text{NS}}|H)$ is written $p(\Lambda_{\text{NS}})$ for brevity. *A priori*, we assume that no particular value of Λ_{NS} is preferred over another within the range [0, 4000], i.e.

$$p(\Lambda_{\text{NS}}|H) = \frac{1}{4000} \text{Rect}\left(\frac{\Lambda_{\text{NS}} - 2000}{4000}\right). \quad (14)$$

With a uniform prior, the first two factors in Eq. (13) can be absorbed into a normalization factor \mathcal{N} , simplifying it to

$$p(\Lambda_{\text{NS}}|d_1, d_2, \dots, d_N; H) = \mathcal{N} \prod_{i=1}^N p(\Lambda_{\text{NS}}|d_i, H). \quad (15)$$

In the second set of terms in Eq. (15) [of the form $p(\Lambda_{\text{NS}}|d_i, H)$], each is the probability distribution for Λ_{NS} inferred *a posteriori* from the i th observation by marginalizing

$$p(\Lambda_{\text{NS}}|d_i, H) = \int p(\vec{\theta}, \Lambda_{\text{NS}}|d_i, H)d\vec{\theta}, \quad (16)$$

734 where $p(\vec{\theta}, \Lambda_{\text{NS}} | d_i, H)$ is the inferred joint probability dis-
 735 tribution of all source parameters $\vec{\theta} \cup \{\Lambda_{\text{NS}}\}$ for the i th event,
 736 as given by Eq. (2). We note that Fig. 5 illustrates
 737 $p(\Lambda_{\text{NS}} | d_i, H)$ for three individual events. By substituting
 738 Eqs. (14)–(16) into Eq. (15), we calculate the probability
 739 distribution for Λ_{NS} as measured using N independent events.

740 Our goal is to understand the improvement in our
 741 measurement of Λ_{NS} with the number of recorded events.
 742 To do so, we simulate a population¹¹ of N events, and
 743 quantify what we learn from each successive observation
 744 using Eq. (15). This allows us to quantify how rapidly our
 745 median estimate for Λ_{NS} converges to the true value, and
 746 how rapidly our credible intervals for the same shrink, with
 747 increasing N . Finally, we generate and analyze an ensemble
 748 of populations in order to average over the stochastic
 749 process of population generation itself.

750 In order to generate each population, the first step is to
 751 fix the NS properties: (i) NS mass $m_{\text{NS}} = 1.35 M_{\odot}$, (ii) NS
 752 spin $\chi_{\text{NS}} = 0$ and (iii) NS tidal deformability $\Lambda_{\text{NS}} =$ fixed
 753 value chosen from $\{500, 800, 1000, 1500, 2000\}$. Next, we
 754 generate events, by sampling BH mass (uniformly) from
 755 $m_{\text{BH}} \in [3 M_{\odot}, 6.75 M_{\odot}]$, BH spin (uniformly) from
 756 $\chi_{\text{BH}} \in [0, 1]$, orbital inclination from $\iota \in [0, \pi]$, and source
 757 location uniform in spatial volume.¹² We restrict ourselves
 758 to positive aligned BH spins, since binaries with anti-
 759 aligned spins have very little information to add at realistic
 760 SNRs, as demonstrated in Fig. 6. This is to be taken into
 761 account when the number of observations is related to
 762 detector operation time. We repeat this process until we
 763 have an ordered set of N events. Since we want to analyze
 764 not just a single realization of an astrophysical population,
 765 but an ensemble of them, we make an additional approxi-
 766 mation to mitigate computational cost. Complete Bayesian
 767 parameter estimation is performed for a set of simulated
 768 signals whose parameters are the vertices of a regular
 769 hypercubic grid (henceforth “G”) in the space of
 770 $\{q\} \times \{\chi_{\text{BH}}\} \times \{\rho\}$, with each sampled at $q = \{2, 3, 4, 5\}$,
 771 $\chi_{\text{BH}} = \{-0.5, 0, 0.5, 0.75\}$, and $\rho = \{10, 20, 30, 50, 70\}$.
 772 All events in each population draw are substituted by their
 773 respective nearest neighbors on the grid G. Our chosen
 774 signal parameter distribution is different from some other
 775 studies in literature, which often sample from more
 776 astrophysically motivated population distribution functions
 777 [99]. We chose one that is sufficiently agnostic in absence
 778 of actual known NSBHs, and pragmatic enough for
 779 generating population ensembles.

780 In Fig. 8 we show illustrative results for a single
 781 population with neutron star deformability $\Lambda_{\text{NS}} = 800$.
 782 In the top panel, each curve shows the probability

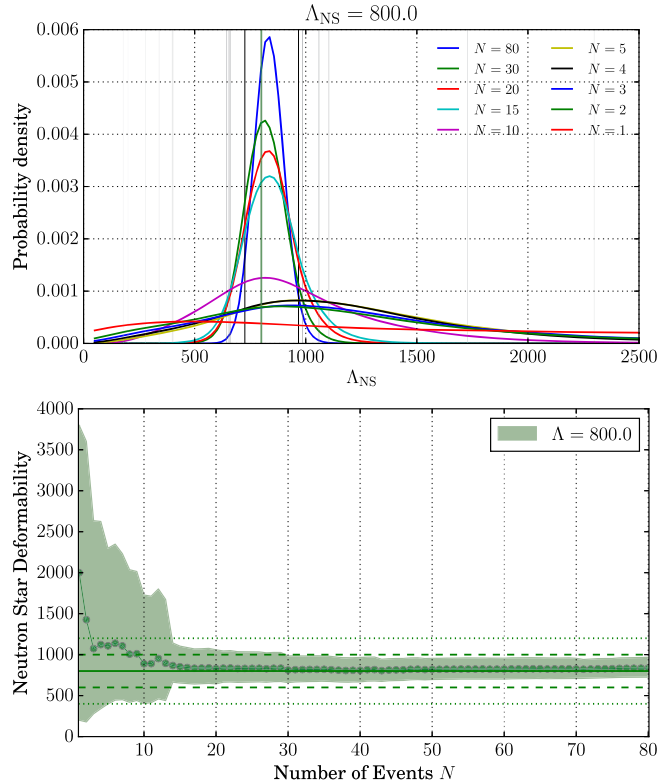


FIG. 8. Recovery of Λ_{NS} for an increasingly large population of BH-NS signals. Top: Posterior probability distributions for Λ_{NS} (colored curves), and associated 90% credible intervals (grey vertical lines), shown for different number of accumulated observations N . Distributions are normalized to unit area. Bottom: Measured median value of Λ_{NS} (as solid circles) and the associated 90% credible intervals (as the vertical extent of filled region), shown as a function of number of observations N . Solid horizontal line indicates the true value of $\Lambda_{\text{NS}} = 800$. Dashed and dotted horizontal lines (a pair for each line style) demarcate $\pm 25\%$ ($\pm 50\%$) error bounds.

distributions for Λ_{NS} as inferred from N events, with N ranging from 1–80. We also mark the 90% credible intervals associated with each of the probability distribution curves. The first few observations do not have enough information to bound Λ_{NS} much more than our prior from Eq. (14) does. In the bottom panel, we present information derived from the top panel. The line-circle curve shows the measured median value from N observations. The pair of dashed (dotted) horizontal lines mark $\pm 25\%$ ($\pm 50\%$) error bars. At each N , the range spanned by the filled region is the 90% credible interval deduced from the same events. This figure somewhat quantifies the qualitative deductions we made from the left panel. We find that the median does track the true value quickly, reaching within its 10% with 10–15 observations. This is as one expects of injections in zero noise where random fluctuations are unable to shift the median away from the true value, so long as the measurement is not restricted by the prior. With the same information, our credible intervals also shrink to $\pm 25\%$. In Fig. 9

¹¹A population here is an ordered set of events, and an event itself is the set of parameters describing one astrophysical NSBH binary.

¹²We distribute sources out to distances where the SNR remains $\rho_{\min} = 10$.

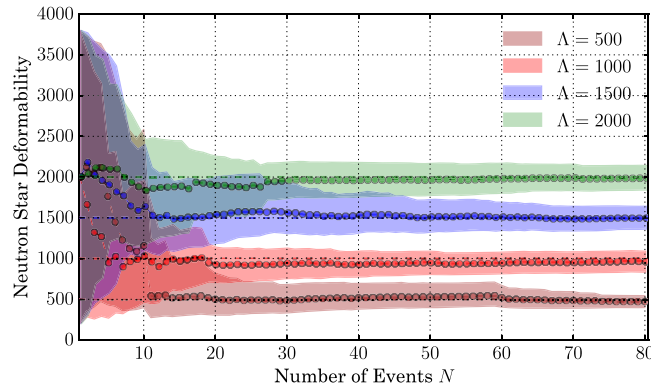


FIG. 9. Improvement in Λ_{NS} measurement accuracy for different NS EoS: In this figure, the filled regions show how our measurement of Λ_{NS} improves as the number of observed events (N , shown on x axis) increases. Each color corresponds to an independent population with its true value of Λ_{NS} given in the legend. For each population, we show the median Λ_{NS} value (as filled circles), as well as the associated 90% credible intervals for the measurement (as the vertical extent of the filled region about the median), as functions of N .

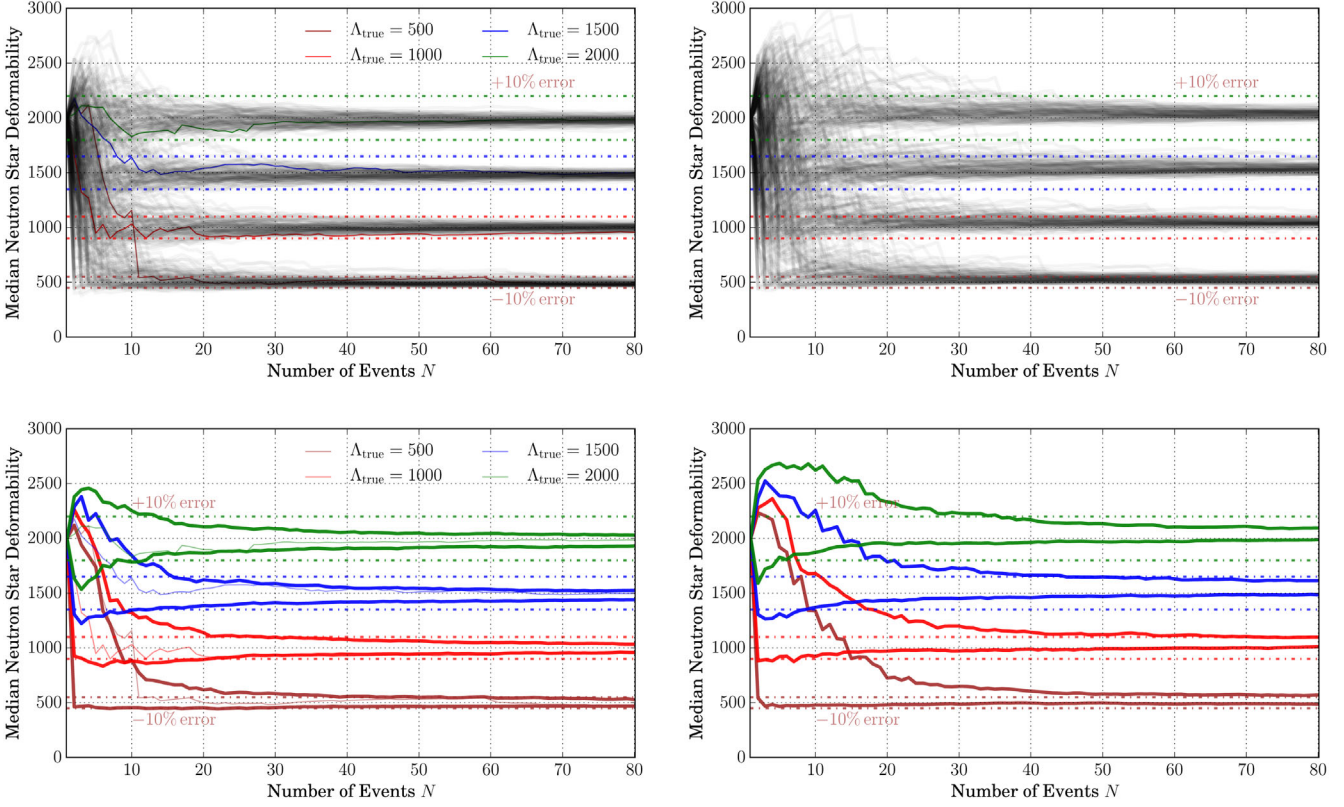
we show further results from four independent populations for $\Lambda_{\text{NS}} = \{500, 1000, 1500, 2000\}$. As in the right panel of Fig. 8, the line-circle curves track the median Λ_{NS} , while the filled regions show the associated 90% credible intervals. From the figure, we observe the following: (i) the shrinkage of credible interval widths with increasing N happens in a similar manner for each Λ_{NS} , and (ii) it takes approximately 20 events to distinguish definitively (with 90% credibility) between deformable NSs with $\Lambda_{\text{NS}} = 2000$ and compact NSs with $\Lambda_{\text{NS}} = 500$, or equivalently to distinguish between hard, moderate and soft nuclear equations of state. This is comparable to what has been found for binary neutron stars [80,83,100].

So far we have discussed individual realizations of NSBH populations. The underlying stochasticity of the population generation process makes it difficult to draw generalized inferences (from a single realization of an NSBH population) about the measurability of Λ_{NS} . In order to mitigate this, we discuss ensembles of population draws next. In Fig. 10 we show the median Λ_{NS} as a function of the number of observed events, for four population ensembles, with a hundred population draws in each ensemble. Let us focus on the *top left* panel first. In it, we show the median Λ_{NS} for all populations in four ensembles, with true $\Lambda_{\text{NS}} = \{2000, 1500, 1000, 500\}$ from top to bottom. Populations highlighted in color are simply those that we discussed in Fig. 9. Dash-dotted horizontal lines demarcate $\pm 10\%$ error intervals around the true Λ_{NS} values. The panel just below it shows the range of Λ_{NS} that encloses the median Λ_{NS} for 90% of the populations in *each* ensemble. In other words, this panel shows the range of Λ_{NS} within which the median Λ_{NS} value for 90% of NSBH populations is expected to lie. From these panels, we observe that our median Λ_{NS} values will be within 10% of the *true* value after ~ 25 detections of less

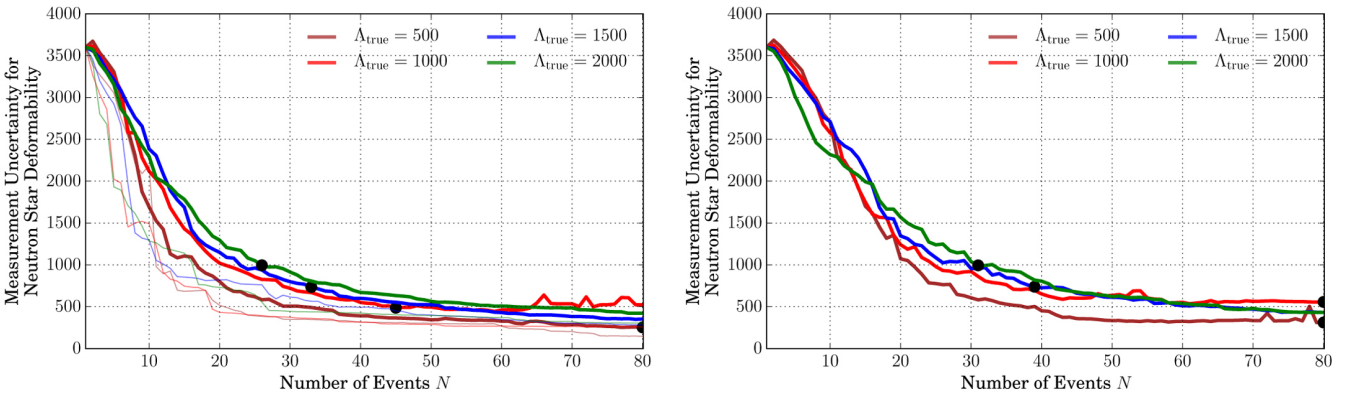
deformable neutron stars ($\Lambda_{\text{NS}} \leq 1000$), or after as few as 15 detections of more deformable neutron stars ($\Lambda_{\text{NS}} \geq 1500$). This is not surprising because we inject simulated signals in *zero* noise, which ensures that the median not be shifted away from the true value. That it takes 15+ events for the median to approach the true value is a manifestation of the fact that the measurement is limited by the prior on Λ_{NS} when we have fewer than 15 events. The results discussed in Figs. 8 and 9 and the left two panels of Fig. 10 apply to the parameter distribution spanned by the grid G. This distribution allows for m_{BH} as low as $2.7 M_{\odot}$ (i.e. $q = 2$). Given that disruptive signatures are strongest for small m_{BH} , we now investigate an alternate paradigm in which no black hole masses fall within the mass gap $2\text{--}5 M_{\odot}$ suggested by astronomical observations [73–76]. We will henceforth denote our standard paradigm, which does not respect the mass gap, as paradigm A, with paradigm B being this alternate scenario. Both right panels of the figure are identical to their corresponding left panels, but drawn under population paradigm B. Under this paradigm, we expectedly find that information accumulation is much slower. It would take 25–40 detections with $\rho \geq 10$ under this paradigm for our median Λ_{NS} to converge within 10% of its true value.

Finally, we investigate the statistical uncertainties associated with Λ_{NS} measurements. We use 90% credible intervals as our measure of the same. First, we draw an ensemble of a hundred populations each for $\Lambda_{\text{NS}} = \{500, 1000, 1500, 2000\}$. For each population i in each ensemble, we construct its 90% credible interval $[\Lambda_{\text{NS},i-}^{90\%}, \Lambda_{\text{NS},i+}^{90\%}]$. Next, we construct the interval $[X^-, Y^-]$ that contains $\Lambda_{\text{NS},i-}^{90\%}$ for 90% of the populations in each ensemble, and similarly $[X^+, Y^+]$ for $\Lambda_{\text{NS},i+}^{90\%}$. Finally, in the left panel of Fig. 11, we show the conservative width $|Y^+ - X^-|$ that contains the 90% credible intervals for 90% of all populations in each ensemble.¹³ From top to bottom, the population Λ_{NS} decreases from $\Lambda_{\text{NS}} = 2000 \rightarrow 500$, corresponding to decreasingly deformable NSs with softer equations of state. We observe the following: (i) for moderately hard to hard equations of state with $\Lambda_{\text{NS}} \geq 1000$, we can constrain Λ_{NS} within $\pm 50\%$ using only 10–20 events, and within $\pm 25\%$ (marked by black circles) with 25–40 events; (ii) for softer equations of state with $\Lambda_{\text{NS}} < 1000$, we will achieve the same accuracy with 20–30 and 50+ events, respectively; and (iii) for the first five or so observations, our measurement spans the entire prior allowed range: $\Lambda_{\text{NS}} \in [0, 4000]$, as shown by the plateauing of the 90% credible intervals towards the left edge to 90% of 4000, i.e. 3600. The right panel in Fig. 11 is identical to the left one, with the difference that populations are drawn under paradigm B, which does *not* allow for BH masses to fall within the mass gap. We find that for NSs with $\Lambda_{\text{NS}} \leq 1000$, it would take 25–40 events to constrain Λ_{NS} within $\pm 50\%$

¹³With source parameters sampled under paradigm A, in which mass-gap is *not* respected.



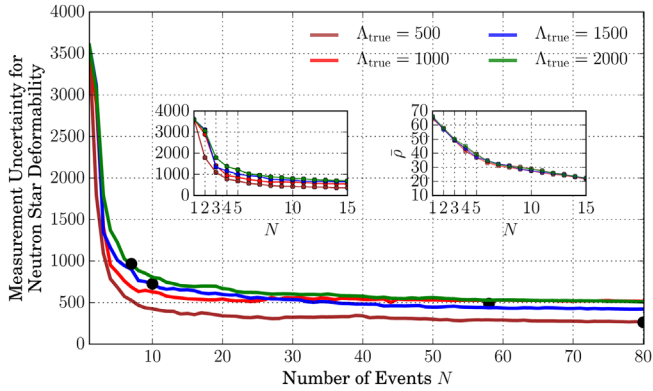
F10:1 FIG. 10. No mass gap, top left: The top figure shows the median value of the recovered probability distribution for Λ_{NS} , as a function
F10:2 of the number of observed events N . There are four ensembles of curves, corresponding to $\Lambda_{\text{NS}} = \{500, 1000, 1500, 2000\}$, with a
F10:3 hundred independent population draws within each ensemble. One curve in each ensemble is highlighted in color, representing the
F10:4 realizations already plotted in Fig. 9. In the same color we show $\pm 10\%$ error bounds on Λ_{NS} with horizontal dash-dotted lines. No mass
F10:5 gap, bottom left: Here we show the interval of Λ_{NS} values within which the median Λ_{NS} lies for 90% of the populations in each ensemble
F10:6 shown in the top left panel. We observe that within 10–25 observations, the median of the measured cumulative probability distribution
F10:7 for Λ_{NS} converges to within 10% of its true value. Mass gap, right column: These panels are identical to their counterparts on the left,
F10:8 with the only difference that the BH masses in each population are restricted to lie *outside* the astrophysical mass gap (i.e. paradigm B).
F10:9 The difference that we observe under this paradigm is that we need more (30+) events to achieve the same (10%) measurement accuracy
F10:10 for populations with $\Lambda_{\text{NS}} < 1000$. For more deformable neutron stars, 10–25 events would suffice.



F11:1 FIG. 11. No mass gap (left): This panel shows the width of the Λ_{NS} interval within which the 90% credible intervals for Λ_{NS} lie, for
F11:2 90% of the populations in each ensemble, as a function of the number of observed events N . Details of how this is calculated are given in
F11:3 the text. The populations are sampled under paradigm A, which allows BH masses to fall within the astrophysical mass gap. Each panel
F11:4 corresponds to a unique value of populations' Λ_{NS} , decreasing from 2000 → 500 as we go from top to bottom. One curve in each
F11:5 ensemble is highlighted in color (thin lines), representing the realizations already plotted in Fig. 9. Mass gap (right): This panel shows
F11:6 populations drawn under paradigm B, which respects the mass gap. We find that with approximately 25 or so events, we begin to put
F11:7 statistically meaningful constraints on Λ_{NS} , restricting it to within $\pm 50\%$ of the true value. We can expect to achieve this with a few years
F11:8 of design aLIGO operation [81]. Further tightening of Λ_{NS} credible intervals will require 40+ events.

and 50+ events to constrain it within $\pm 25\%$. This is somewhat slower than paradigm A, as is to be expected since here we preclude the lowest mass ratios, which correspond to signals with largest tidal signatures. For $\Lambda_{\text{NS}} > 1000$ we find that we can constrain Λ_{NS} within $\pm 50\%$ with a similar number of events as for paradigm A, but will need more (30–40 as compared to 25–40) events to further constrain it to within $\pm 25\%$ of the true value. Under either paradigms, we find that measuring Λ_{NS} better than 25% will require $\mathcal{O}(10^2)$ observations of disruptive NSBH mergers. These results demonstrate that our probed set of disruptive NSBH mergers is as informative of NS tidal properties as are BNS populations, if we assume a uniform mass distribution for NSs and zero NS spins, and possibly more if NS masses are not distributed uniformly [83]. However, being a subset of all NSBH binaries, the accumulation of information from NSBH signals in general may be slower than from binary neutron stars, depending on the distribution of BH masses in coalescing NSBH binaries.

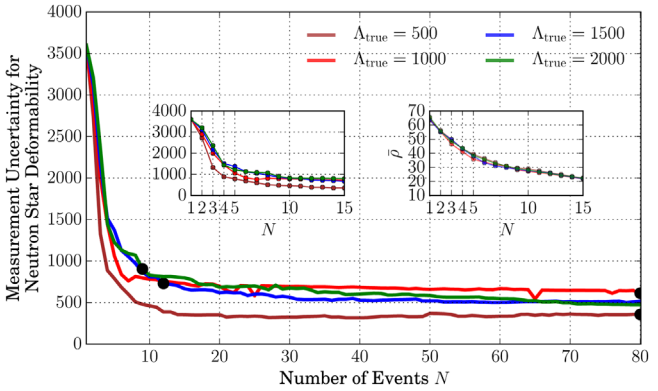
Do all events matter? In Ref. [60] the authors demonstrate that the overwhelming majority of information about the NS equation of state comes from the loudest ~ 5 events in the case of binary neutron star detections, and not from the combined effect of a large number of low-SNR systems. The question naturally arises if the same is true for NSBH sources as well. Therefore, in Fig. 12 we reevaluate the accumulation of information with each successive NSBH detection, sorting the events in each population by their SNR instead of simulated chronology. We find the same qualitative behavior as in the case of BNSs [60]. Whether or not there is an astrophysical mass gap, we find that the bulk of tidal information will be furnished by the loudest 5–10 NSBH detections of aLIGO detectors. This result is especially encouraging to NR follow-up efforts for GW detections, as we now know that only a handful of loudest NSBH events (with SNRs $\rho \gtrsim 20$ –30) are the ones that may merit full numerical-GR + magnetohydrodynamical follow-up simulations.



To summarize, in this section we study the improvement in our measurement of NS deformability parameter Λ_{NS} with an increasing number of events. We do so by simulating plausible populations of disrupting NSBH binaries (with $\rho \geq 10$). We find that: (i) for more deformable neutron stars (harder equation of states), the median value of Λ_{NS} comes within 10% of the true value with as few as 10 events, while achieving the same accuracy for softer equations of state will take 15–20 source detections; (ii) the statistical uncertainty associated with Λ_{NS} measurement shrinks to within $\pm 50\%$ with 10–20 events, and to within $\pm 25\%$ with 50+ events, when source $\Lambda_{\text{NS}} \geq 1000$; (iii) for softer equations of state, the same could take 25–40 and 50+ events, respectively for the two uncertainty thresholds; and (iv) if BHs really do observe the astrophysical mass gap, the information accumulation is somewhat slower than if they do not. We conclude that within 20–30 observations, aLIGO would begin to place very interesting bounds on the NS deformability, which would allow us to rule out or rank different equations of state for neutron star matter. Within this population, we also find that it will be the loudest 5–10 events that will furnish most of the tidal information. Our key findings are summarized in Figs. 10–12.

VI. DISCUSSION

The pioneering observation of gravitational waves by Advanced LIGO harbinger the dawn of an era of gravitational-wave astronomy where observations would finally drive scientific discovery [101]. As confirmed by the first observations [18,101,102], stellar-mass compact binary mergers emit GWs right in the sensitive frequency band of the LIGO observatories, and are their primary targets. Neutron star-black hole binaries form a physically distinct subclass of compact binaries. We expect to detect the first of them in the upcoming observing runs [103], and



F12:1 FIG. 12. This figure is similar to Fig. 11, with the only difference being that events in each population have been sorted according to their signal strength (SNR), instead of their simulated chronology. We note that information about the tidal deformability of neutron stars comes primarily from the loudest 5–10 events, whether we allow BH masses in the mass gap (left panel) or restrict them to $m_{\text{BH}} \geq 5 M_{\odot}$ (right panel). The left inset zooms in on the main figure for the first 15 events. The right inset shows the actual (ensemble mean) SNR value for each event. We find that events with $\rho \gtrsim 20$ –30 provide the bulk of tidal information in our analysis.
F12:2
F12:3
F12:4
F12:5

subsequently at a healthy rate of 0.2–300 mergers a year when ALIGO detectors reach design sensitivity [31].

NSBH binaries are interesting for various reasons. Unlike BBHs, the presence of matter allows for richer phenomena to occur alongside the strong-field gravitational dynamics. The quadrupolar moment of the NS changes during the course of inspiral, which increases the inspiral rate of the binary and alters the form of the emitted gravitational waves. Close to merger, under restricted but plausible conditions, the neutron star is disrupted by the tidal field of its companion black hole and forms an accretion disk around it. This disruption reduces the quadrupolar moment of the system, and decreases the amplitude of the emitted GWs from the time of disruption through to the end of ringdown. Both of these phenomena are discernible in their gravitational-wave signatures alone. In addition, if the neutron star matter is magnetized, the magnetic winding above the remnant black hole poles can build up magnetic fields sufficiently to power short gamma-ray bursts (SGRB) [38,39,41–44]. Therefore a coincident observation of gravitational waves from an NSBH merger and a SGRB can potentially confirm the hypothesis that the former is a progenitor of the latter [32–40].

In this paper we study the observability of tidal signatures in the gravitational-wave spectrum of NSBH binaries. More specifically, we investigate three questions. First, what is the effect of not including tidal effects in templates while characterizing NSBH signals? Second, if we do include tidal effects, how well can we measure the tidal deformability of the NS (parametrized by Λ_{NS}) from individual NSBH signals? Third, as we observe more and more signals, how does our knowledge of Λ_{NS} improve? In the following, we summarize our main findings.

First, we study the effects of not including tidal terms in our search templates while characterizing NSBH signals. We expect that the waveform template that best fits the signal would compensate for the reduced number of degrees of freedom in the template model by moving away from the true parameters of the binary. This should result in a *systematic* bias in the recovered values of nontidal source parameters, such as its masses and spins. In order to quantify it, we inject tidal signals into zero noise, and perform a Bayesian parameter estimation analysis on them using templates *without* tidal terms. We use the LEA+ model (cf. Sec. II A) to produce tidal waveforms that incorporate the effect of NS distortion during inspiral, and of its disruption close to merger. Our injected signals sample the region of NSBH parameter space where NS disruption prior to binary merger is likely *and* can be modeled using LEA+. Their parameters are given by combinations of $q = m_{\text{BH}}/m_{\text{NS}} = \{2, 3, 4, 5\}$, $\chi_{\text{BH}} = \{-0.5, 0, 0.5, 0.75\}$ and $\Lambda_{\text{NS}} = \{500, 800, 1000, 1500, 2000\}$. Other parameters, such as source location and orientation, that factor out of $h(t)$ as amplitude scaling are cosampled by varying $\rho = \{20, 30, 50, 70\}$.

At low to moderate SNRs ($\rho \lesssim 30$), we find that using BBH templates does not significantly hamper our estimation of nontidal parameters for NSBH signals. In the worst case, when the BH mass is within the astrophysical mass gap [73–76] and its spin is positive aligned, the systematic biases in η and χ_{BH} measurements do become somewhat comparable to statistical errors (ratio ~ 0.5 – 0.8) under very restrictive conditions,¹⁴ but never exceed them. At high SNRs ($\rho \gtrsim 50$), systematic biases in \mathcal{M}_c become larger than the statistical uncertainties. For η and χ_{BH} the difference is more drastic with the systematics reaching up to $4\times$ the statistical errors. We therefore conclude that $\rho \simeq 30$ – 50 is loud enough to motivate the use of tidal templates for even the estimation of nontidal parameters from NSBH signals. We also conclude that low-latency parameter estimation algorithms, designed to classify GW signals into electromagnetically active (NSBH and NSNS) and inactive (BBH) sources, can use BBH templates to trigger GRB alerts [50,104–108] for NSBH signals with low to moderate SNRs ($\rho \lesssim 30$). This is so because the primary requirement of identifying NS-X binaries ($X = \{\text{NS}, \text{BH}\}$) can be achieved just as easily with BBH templates, on the basis of the smaller component's mass.¹⁵ We also speculate that NSBH detection searches are unlikely to be affected by the choice of ignoring tidal effects in matched-filtering templates, if these effects are too subtle to manifest in parameter estimation below $\rho \simeq 30$.

Second, we turn the question around to ask: can we measure the tidal effects if our template models did account for them? Tidal effects in our waveform model are parametrized using a single deformability parameter $\Lambda_{\text{NS}} \propto (R/M)_{\text{NS}}^5$. In order to quantify the measurability of Λ_{NS} , we inject the same tidal signals as before, and this time perform a Bayesian analysis on them using *tidal* templates. The results are detailed in Sec. IV. At low SNRs ($\rho \simeq 20$), we find that the best we can do is to constrain Λ_{NS} within $\pm 75\%$ of its true value at 90% credible level; this too only if the BH is spinning sufficiently rapidly, with $\chi_{\text{BH}} \gtrsim +0.7$, and the NS has $\Lambda_{\text{NS}} \gtrsim 1000$. At moderate SNRs ($\rho \simeq 30$), we can constrain Λ_{NS} a little better, i.e. within $\pm 50\%$ of its true value. This level of accuracy, however, again requires that BH spin $\chi_{\text{BH}} \gtrsim +0.7$ and $\Lambda_{\text{NS}} \gtrsim 1000$. Binaries with smaller BH spins and/or softer NS EoSs will furnish worse than $\pm 75\% - \pm 100\%$ errors for Λ_{NS} . This trend continues as we increase the SNR from $\rho = 30$ – 50 . It is not until we reach an SNRs as high as $\rho \simeq 70$ that we can shrink Λ_{NS} errors substantially with a single observation (i.e. within $\pm 25\%$ of its true value). In summary, we find that with a single but moderately loud

¹⁴Those conditions being: a companion BH with mass $m_{\text{BH}} \lesssim 4.5 M_{\odot}$ (i.e. in the astrophysical mass-gap), and the *hardest* NS EoS amongst those considered in this work (with $\Lambda_{\text{NS}} \simeq 2000$).

¹⁵The smaller component mass is unlikely to be significantly biased by missing tidal effects in filter templates below $\rho \simeq 30$, as we show above.

1064 NSBH signal, Advanced LIGO can begin to put a factor of
 1065 $1\text{--}2\times$ constraints on the NS tidal deformability parameter.
 1066 These constraints can subsequently be used to assess the
 1067 likelihood of various candidate equations of state for
 1068 nuclear matter, and possibly to narrow the range they span.

1069 Third, knowing that single observations can furnish only
 1070 so much information about the NS equation of state, we
 1071 move on to investigate how well we do with multiple
 1072 signals. In order to quantify how Λ_{NS} measurement
 1073 improves with the number of observed events N , we
 1074 generate populations of NSBH signals and combine the
 1075 information extracted from each event. The population
 1076 generation procedure is as follows. The neutron star mass is
 1077 held fixed at $1.35 M_{\odot}$, its spin at $\chi_{\text{NS}} = 0$, and its tidal
 1078 deformability is fixed to each of $\Lambda_{\text{NS}} = \{500, 1000, 1500,$
 1079 $2000\}$. Black hole mass is sampled uniformly from the
 1080 range $[2, 5] \times 1.35 = [2.7, 6.75] M_{\odot}$, and spin from
 1081 $\chi_{\text{BH}} \in [0, 1]$. As before, our parameter choice here is given
 1082 by the intersection set of the mass range that allows for
 1083 neutron star disruption and the range supported by LEA+
 1084 [[44,65,109](#)]. In order to keep the computational cost
 1085 reasonable, we make an additional approximation. For
 1086 every population generated, we replace the parameters of
 1087 each event by their nearest neighbor on the uniform grid G ,
 1088 which has vertices at $q = \{2, 3, 4, 5\} \times \chi_{\text{BH}} = \{-0.5, 0,$
 1089 $0.5, 0.75\} \times \Lambda_{\text{NS}} = \{500, 800, 1000, 1500, 2000\} \times \rho = \{10,$
 1090 $20, 30, 50, 70\}$. This way, we only have to run full Bayesian
 1091 parameter estimation analysis on this fixed set of signals.
 1092 There are two sources of error that enter the deductions we
 1093 make from a single population generated in the manner
 1094 described above. First, since the injection parameters are
 1095 pushed to their nearest neighbor on a grid, we find discrete
 1096 jumps in Λ_{NS} errors as a function of N . Second, an individual
 1097 population is one particular realization of a stochastic
 1098 process and could have excursions that may never be found
 1099 in another population. To account for both of these limitations,
 1100 we generate an ensemble of populations, and
 1101 conservatively combine information from all of them.¹⁶

1102 We probe two astrophysical paradigms, one that allows for
 1103 BH masses to lie within the astrophysical mass gap (para-
 1104 digm A), and one that does not (paradigm B). *For paradigm*
 1105 *A*, we find the following: (i) for the softer equations of state
 1106 that result in less deformable neutron stars, 15–20 detections
 1107 bring the measured probability distribution for Λ_{NS} entirely
 1108 within the prior, which ensures that the median Λ_{NS} tracks
 1109 the true value to within 10%. (ii) For NSBH populations with
 1110 more deformable NSs ($\Lambda_{\text{NS}} > 1000$), the same is achievable
 1111 within as few as 10 (or 15 at most) realistic observations.
 1112 (iii) The statistical uncertainty associated with Λ_{NS} mea-
 1113 surement can be restricted to be within $\pm 50\%$ using 10–20
 1114 observations when $\Lambda_{\text{NS}} > 1000$, and using 25–40 obser-
 1115 vations for softer equations of state. All of the above is
 1116 possible within a few years of design aLIGO operation [[81](#)],

if astrophysical BHs are allowed masses $< 5 M_{\odot}$ (i.e. in the
 mass gap). However, further restricting Λ_{NS} will require 50+
 NSBH observations. *For paradigm B*, we find the information
 accumulation to be somewhat slower. While the quantitative
 inferences for populations with $\Lambda_{\text{NS}} > 1000$ are not affected significantly, we find that $\Lambda_{\text{NS}} < 1000$
 populations require 10%–20% more events to attain the
 same measurement accuracy as under paradigm A. In either
 case, the accumulation of information from the general
 NSBH population will likely be slower than from BNS
 inspirals [[60,61,83,99](#)], depending on the mass distribution
 of stellar-mass black holes. Though, template models for the
 latter may be more uncertain due to missing point-particle
 PN terms at orders comparable to tidal terms [[60](#)]. We
 conclude that within as few as 20–30 observations of
 disruptive NSBH mergers, aLIGO will begin to place
 interesting bounds on NS deformability. This, amongst other
 things, will allow us to rank different equations of state for
 neutron star matter from most to least likely, within a few
 years' detector operation. We also find that, within this
 population, the loudest 5–10 events (with SNRs $\rho \gtrsim 20$ –30)
 will provide us with most of the tidal information, and will
 therefore merit full NR follow-up. Our methods and results
 are detailed in Sec. V.

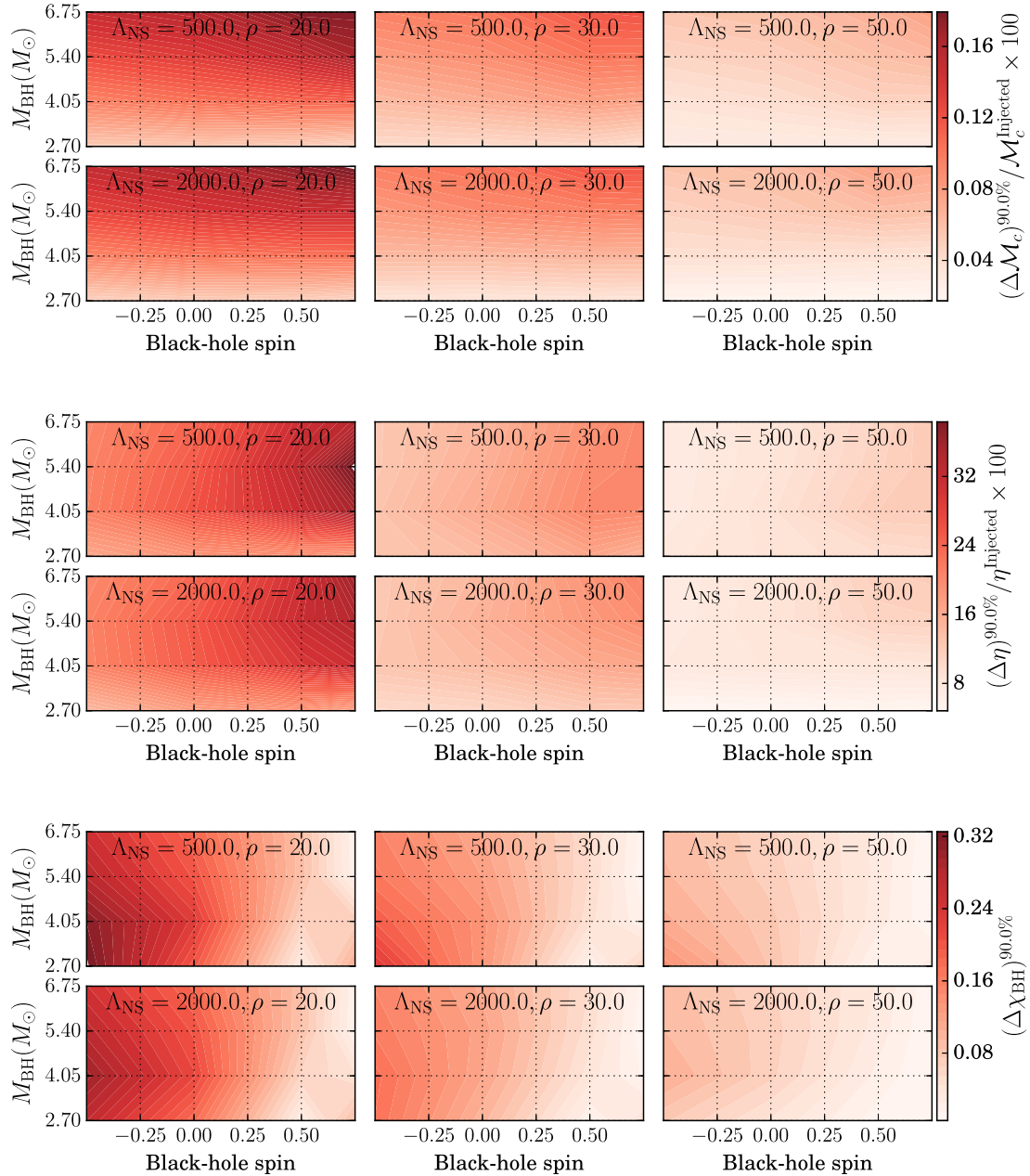
Finally, we note that the underlying numerical simulations
 used to calibrate the waveform model used here have
 not been verified against independent codes so far. It is
 therefore difficult to assess the combined modeling error of
 LEA+ and its effect on our results. Our results here are,
 therefore, limited by the limitations of our waveform model,
 and presented with this caveat. However, we do expect the
 combined effect of modeling errors to *not* affect our
qualitative conclusions, especially since the underlying
 point-particle component of LEA+ includes all high-order
 terms, unlike past BNS studies [[60,61](#)]. In the future, we plan
 to further the results presented here by using more recent
 tidal models [[82,110](#)], which may improve upon LEA+.¹⁷

ACKNOWLEDGMENTS

We thank Benjamin Lackey, Francesco Pannarale,
 Francois Foucart, and Duncan Brown for helpful discussions.
 We gratefully acknowledge support for this research
 at CITA from Natural Sciences and Engineering Research
 Council of Canada (NSERC), the Ontario Early Researcher
 Awards Program, the Canada Research Chairs Program, and
 the Canadian Institute for Advanced Research. Calculations
 were performed at the Vulcan supercomputer at the Albert
 Einstein Institute; H. P. and P. K. thank the Albert-Einstein
 Institute, Potsdam, for hospitality during part of the time
 where this research was completed. M. P. thanks CITA for
 hospitality where part of the work was carried out.

¹⁶See Sec. V for further details.

¹⁷One of them [[82](#)] is only an amplitude model though, which
 has to be augmented with a compatible phase model first.



F13:1
F13:2 FIG. 13. Statistical measurement uncertainty for NSBH parameters, ignoring tidal effects: We show here the statistical uncertainty
F13:3 associated with our measurement of nontidal parameters \mathcal{M}_c , η , and χ_{BH} (at 90% credibility), over the signal parameter space. Individual
F13:4 panels show the same as a function of BH mass and spin. Across each row, we see the effect of increasing signal strength (i.e. SNR) with
F13:5 the tidal deformability of the NS Λ_{NS} fixed. Down each column, we see the effect of increasing Λ_{NS} , at fixed SNR. Tidal effects are
ignored in templates.

APPENDIX A: STATISTICAL UNCERTAINTY IN MEASURING NONTIDAL PARAMETERS

In Fig. 13, we show how precisely can we measure nontidal NSBH parameters $X = \{\mathcal{M}_c, \eta, \chi_{\text{BH}}\}$ using BBH templates. The three panels correspond to \mathcal{M}_c (top), η (middle), and χ_{BH} (bottom), and show the width of these credible intervals $(\Delta X)^{90\%}$ as a function of BH mass/spin (within each subpanel), and NS properties, i.e. Λ_{NS}

(downwards in each column).¹⁸ From the leftmost column, we find that: (i) at $\rho = 20$ the chirp mass is measured remarkably well—to a precision of 0.16% of its true value,

¹⁸We restrict NS mass to $1.35 M_\odot$ and its spin to zero. Varying its tidal deformability Λ_{NS} does not significantly change the measurement uncertainties for nontidal binary parameters, as is evident from comparing the two rows in each panel of Fig. 13.

and (ii) so is χ_{BH} . (iii) The dimensionless mass ratio η is determined more loosely, with 25 + % uncertainty. If the signal is even louder ($\rho \geq 30$), all three measurements gain further precision, especially η , for which the relative errors shrink down to single-digit percents. We remind ourselves that these results do not tell the full story since the precision of a measurement is only meaningful if the measurement is accurate to begin with. In our case there are tidal effects that have not been incorporated into our search (BBH) templates, which can lead to a systematic bias in parameter recovery. We refer the reader to Sec. III for a comparative study of both systematic and statistical errors.

APPENDIX B: ILLUSTRATIONS OF BAYESIAN POSTERIORS

In Fig. 14 we show the correlation of mass, spin, and tidal parameter measurements. We keep the binary parameters as in Fig. 5, with $\Lambda_{\text{NS}} = 2000$, and set $\rho = 20$ (left panel) or $\rho = 50$ (right panel). We find that the measurement of Λ_{NS} is weakly degenerate with other parameters, and at realistic SNRs it would improve by a few tens of percent if we knew nontidal parameters to better accuracy. The predominant factor that would enhance the measurement accuracy for Λ_{NS} is nevertheless the signal strength. Only when $\rho \gtrsim 50$ can we expect Λ_{NS} measurement to be limited by its

degeneracy with nontidal parameters (at a factor of few level), as also reported by previous studies [65].

APPENDIX C: PHENOMENOLOGY OF Λ_{NS} MEASUREMENT ERRORS

Here, we quantitatively explore the dependence of our statistical uncertainties for Λ_{NS} on the number of events, as well as on the true NS deformability itself. First, we will focus on the dependence on N . We assume a power-law dependence of the form $\delta\Lambda_{\text{NS}} \propto 1/N^\alpha$. For each of the 100 populations for each of $\Lambda_{\text{NS}} = 500\text{--}2000$, we compute the exponent α as a function of the number of observed events N , and show it in Fig. 15. There are $100 \times 5 = 500$ curves on the figure, with one highlighted for each value of the population's Λ_{NS} . These highlighted values are only special in the sense that they correspond to populations discussed earlier in this section (cf. Figs. 8 and 9). We immediately observe two things: (i) there is a globally similar dependence on N for all populations, and (ii) information accumulates faster than $1/\sqrt{N}$. In fact, we find that if $\delta\Lambda_{\text{NS}} \propto \frac{1}{N^\alpha}$, α lines in the range $0.7^{+0.2}_{-0.2}$. Next, we focus on the dependence of $\delta\Lambda_{\text{NS}}$ on Λ_{NS} of the population itself. As suggested by Fisher-matrix studies [65], and as for N , we assume the form $\delta\Lambda_{\text{NS}} \propto \Lambda_{\text{NS}}^\beta$. From each set of 100 populations with a given Λ_{NS} value, we draw one at random, and form a set of five

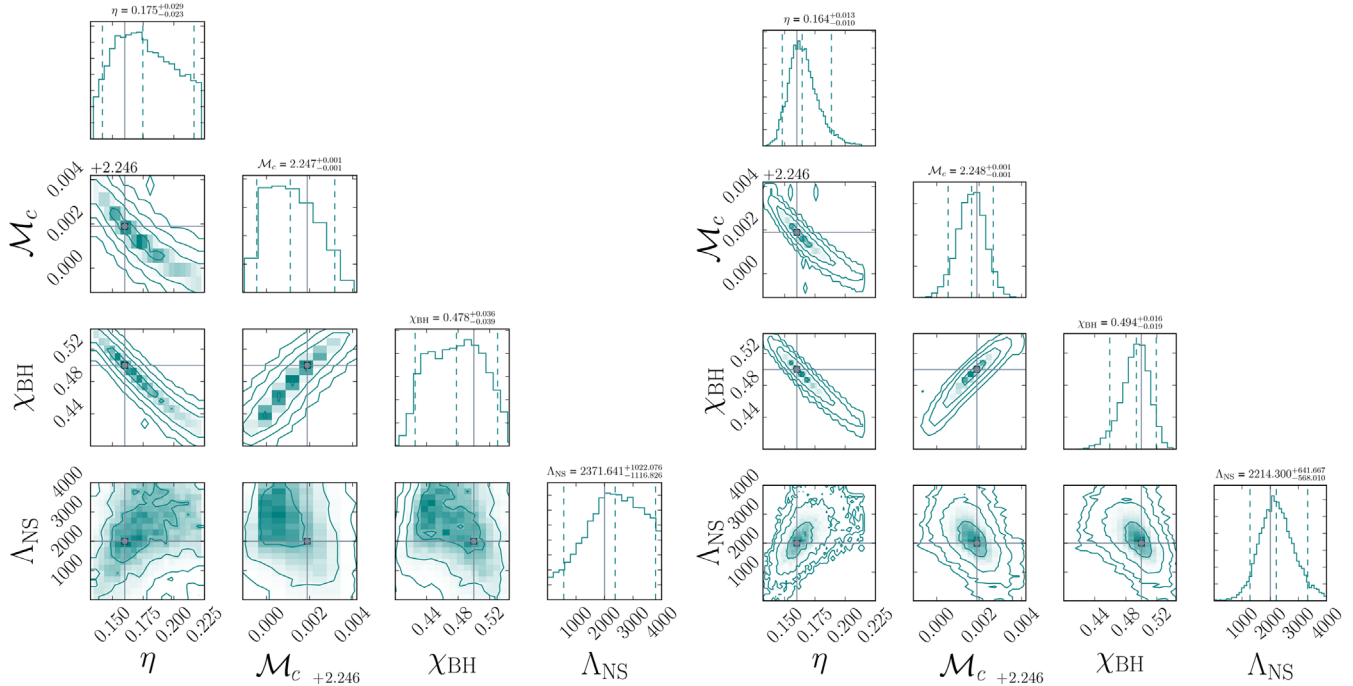


FIG. 14. Illustrative posterior probability distributions for NSBH parameters, for signals at different SNRs: We illustrate here two sets of two-dimensional joint probability distributions, differing only in signal strength, with $\rho = 20$ in the left panel, and $\rho = 50$ in the right. The injected parameters are $q = m_{\text{BH}}/m_{\text{NS}} = 5.4 M_\odot/1.35 M_\odot = 4$, $\chi_{\text{BH}} = +0.5$, and $\Lambda_{\text{NS}} = 2000$. Contours are shown for $\{1-, 2-, 3-, \dots\}\sigma$ confidence levels. Templates include tidal effects, as evident in the bottom rows of both panels which show the correlation of Λ_{NS} with nontidal parameters. Contrasting the two panels illustrates the effect of increasing the SNR on various parameter measurements.

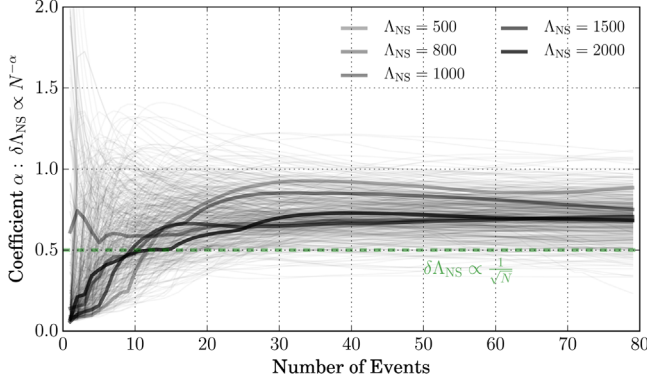


FIG. 15. Assuming a power-law dependence of the measurement error on the number of events: $\delta\Lambda_{\text{NS}} \propto 1/N^\alpha$, we show α in this figure as a function of the number of observed events N . Shown are five families of 100 population draws each, with each family corresponding to one of $\Lambda_{\text{NS}} = \{500, 800, 1000, 1500, 2000\}$. Each grey curve corresponds to one of these $100 \times 5 = 500$ populations. The thicker curves, one from each family, show the population we discussed in Figs. 8 and 9. We find that a power law is a good approximation for the concerned dependence, and information accumulates *faster* than $1/\sqrt{N}$. We estimate $\alpha = 0.7^{+0.2}_{-0.2}$.

similarly drawn populations, one for each of $\Lambda_{\text{NS}} = \{500, 800, 1000, 1500, 2000\}$. With each set, we determine β for a different number of observed events N . In all, we make 100 independent five-population sets and show the value of β measured from each in Fig. 16. We find that the assumed relation $\delta\Lambda_{\text{NS}} \propto \Lambda_{\text{NS}}^\beta$ gets fairly robust for larger values of N , with β converging to $0.5^{+0.33}_{-0.33}$. The fact that $0 < \beta < 1$ implies that the relative error $\delta\Lambda_{\text{NS}}/\Lambda_{\text{NS}}$

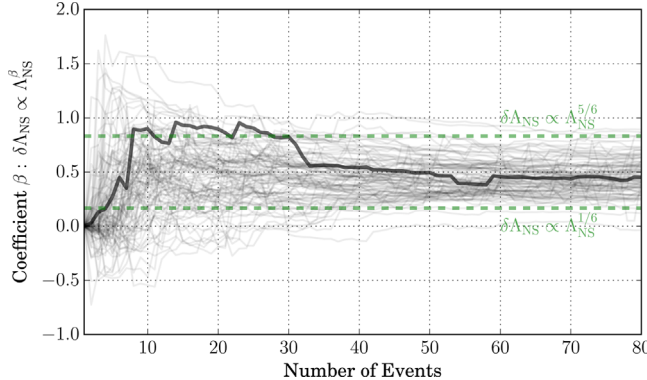


FIG. 16. In this figure, which is similar to Fig. 15, we quantify the dependence of $\delta\Lambda_{\text{NS}}$ on Λ_{NS} itself. Of the five families of simulated NSBH populations, we construct 100 independent sets taking one population from each family. With each of these 100 sets, and assuming a power-law dependence: $\delta\Lambda_{\text{NS}} \propto \Lambda_{\text{NS}}^\beta$, we estimate β and show it in this figure as a function of the number of observed events N . The thicker curve corresponds to the populations discussed in Fig. 9. We find that β can be estimated to lie within $[1/6, 5/6]$ with a likely value close to $1/2$. Since $0 < \beta < 1$, the relative error $\delta\Lambda_{\text{NS}}/\Lambda_{\text{NS}}$ decreases as the star gets more deformable, while the absolute error $\delta\Lambda_{\text{NS}}$ increases.

decreases with increasing Λ_{NS} , while the absolute error increases. From these results, we conclude that the measurement uncertainty for Λ_{NS} after N observations is

$$\delta\Lambda_{\text{NS}} \propto \frac{\Lambda_{\text{NS}}^{0.5^{+0.33}_{-0.33}}}{N^{0.7^{+0.2}_{-0.2}}} \quad (\text{C1})$$

We also find that while these results are inferred from paradigm A populations, paradigm B gives very similar results.

APPENDIX D: CHOICE OF UNDERLYING BBH MODEL IN LEA

The waveform model used in this paper is a variant of those calibrated in Ref [65]. In that work, the authors also calibrate a tidal prescription with the phenomenological model IMRPhenomC [111] as the base BBH model. Previous work [88,89] has shown that IMRPhenomC can exhibit pathological behavior for mass ratios $q \gtrsim 4$ and/or nonzero black hole spins. We compute noise-weighted inner products between the two variants for 2,000,000 points sampled over the NSBH parameter space, and show the results in Fig. 17. We restrict the comparison to frequencies that are affected by the tidal disruption of the NS, by integrating the inner products from $f = \max(15, 0.01/M)$ Hz {where M is expressed in seconds [$1 M_\odot \simeq 4.925\mu\text{s}$, see Eqs. (32)–(34) of [65]]}. We find that the differences between the two variants of LEA+ have mismatches of a few percent, while the tidal corrections contribute at a subpercent level. We conclude that the differences of the underlying BBH model in LEA+ dominate over its tidal calibration, and since SEOBNRv2 has been shown to be more reliable than IMRPhenomC [88,89], we recommend the use of SEOBNRv2-based LEA+ in upcoming LIGO-Virgo analyses.

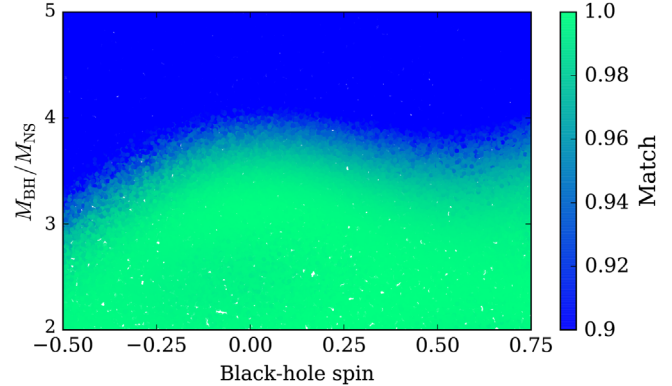


FIG. 17. We compare two alternatives of the tidal NSBH model from Ref. [65], which differ in their underlying BBH prescriptions. One which we use in this study uses SEOBNRv2, while the other uses IMRPhenomC as its base. In this figure, we show the normalized overlap (match) between the two for 2,000,000 points sampled uniformly in the NSBH parameter space. We find that for $q \gtrsim 4$ the discrepancies between IMRPhenomC and SEOBNRv2 as reported in [88] dominate over tidal terms.

- 1263 [1] D. Shoemaker (LIGO Collaboration), Advanced LIGO
1264 anticipated sensitivity curves, LIGO Document
1265 No. T0900288-v3, 2010.
- 1266 [2] B. P. Abbott *et al.* (LIGO Scientific Collaboration, Virgo
1267 Collaboration), *Phys. Rev. Lett.* **116**, 061102 (2016).
- 1268 [3] F. Acernese *et al.* (Virgo Collaboration), *Classical Quantum
1269 Gravity* **32**, 024001 (2015).
- 1270 [4] Y. Aso, Y. Michimura, K. Somiya, M. Ando, O. Miyakawa,
1271 T. Sekiguchi, D. Tatsumi, and H. Yamamoto (KAGRA
1272 Collaboration), *Phys. Rev. D* **88**, 043007 (2013).
- 1273 [5] K. Somiya (KAGRA Collaboration), *Classical Quantum
1274 Gravity* **29**, 124007 (2012).
- 1275 [6] C. S. Unnikrishnan, *Int. J. Mod. Phys. D* **22**, 1341010
1276 (2013).
- 1277 [7] F. X. Timmes, S. E. Woosley, and T. A. Weaver, *Astrophys.
1278 J.* **457**, 834 (1996).
- 1279 [8] C. L. Fryer, *Astrophys. J.* **522**, 413 (1999).
- 1280 [9] S. E. Woosley, A. Heger, and T. A. Weaver, *Rev. Mod.
1281 Phys.* **74**, 1015 (2002).
- 1282 [10] K. Belczynski, T. Bulik, C. L. Fryer, A. Ruiter, F.
1283 Valsecchi, J. S. Vink, and J. R. Hurley, *Astrophys. J.*
1284 **714**, 1217 (2010).
- 1285 [11] K. Belczynski, M. Dominik, T. Bulik, R. O’Shaughnessy,
1286 C. Fryer, and D. E. Holz, *Astrophys. J. Lett.* **715**, L138
1287 (2010).
- 1288 [12] M. Dominik, E. Berti, R. O’Shaughnessy, I. Mandel, K.
1289 Belczynski, C. Fryer, D. Holz, T. Bulik, and F. Pannarale,
1290 *Astrophys. J.* **806**, 263 (2015).
- 1291 [13] K. Belczynski, V. Kalogera, F. A. Rasio, R. E. Taam, and T.
1292 Bulik, *Astrophys. J.* **662**, 504 (2007).
- 1293 [14] C. L. Fryer, K. Belczynski, G. Wiktorowicz, M. Dominik,
1294 V. Kalogera, and D. E. Holz, *Astrophys. J.* **749**, 91 (2012).
- 1295 [15] N. Wex and S. Kopeikin, *Astrophys. J.* **514**, 388 (1999).
- 1296 [16] R. Narayan, T. Piran, and A. Shemi, *Astrophys. J.* **379**, L17
1297 (1991).
- 1298 [17] I. Mandel, C.-J. Haster, M. Dominik, and K. Belczynski,
1299 *Mon. Not. R. Astron. Soc.* **450**, L85 (2015).
- 1300 [18] B. P. Abbott *et al.* (Virgo, LIGO Scientific), *Astrophys. J.*
1301 **833**, L1 (2016).
- 1302 [19] D. Psaltis *et al.*, in *Compact Stellar X-ray Sources*, edited
1303 by M. v. d. K. Walter Lewin (Cambridge University Press,
1304 Cambridge, 2010), p. 708.
- 1305 [20] R. A. Remillard and J. E. McClintock, *Annu. Rev. Astron.
1306 Astrophys.* **44**, 49 (2006).
- 1307 [21] T. Fragos, M. Tremmel, E. Rantsiou, and K. Belczynski,
1308 *Astrophys. J.* **719**, L79 (2010).
- 1309 [22] R. N. Manchester, G. B. Hobbs, A. Teoh, and M. Hobbs,
1310 *Astron. J.* **129**, 1993 (2005).
- 1311 [23] J. M. Lattimer, *Annu. Rev. Nucl. Part. Sci.* **62**, 485 (2012).
- 1312 [24] B. Margon, M. Lampton, S. Bowyer, and R. Crude, *Astrophys.
1313 J. Lett.* **169**, L23 (1971).
- 1314 [25] H. E. Bond, R. L. White, R. H. Becker, and M. S. O’Brien,
1315 *Publ. Astron. Soc. Pac.* **114**, 1359 (2002).
- 1316 [26] R. A. Hulse and J. H. Taylor, *Astrophys. J.* **195**, L51
1317 (1975).
- 1318 [27] J. H. Taylor and J. M. Weisberg, *Astrophys. J.* **253**, 908
1319 (1982).
- 1320 [28] J. Weisberg, D. Nice, and J. Taylor, *Astrophys. J.* **722**,
1321 1030 (2010).
- [29] H.-T. Janka, T. Eberl, M. Ruffert, and C. L. Fryer,
Astrophys. J. **527**, L39 (1999). 1322
- [30] C. L. Fryer, F. G. Oliveira, J. A. Rueda, and R. Ruffini,
Phys. Rev. Lett. **115**, 231102 (2015). 1323
- [31] J. Abadie, B. P. Abbott, R. Abbott, M. Abernathy, T.
Accadia, F. Acernese, C. Adams, R. Adhikari, P. Ajith,
B. Allen *et al.* (LIGO Scientific Collaboration, Virgo
Collaboration), *Classical Quantum Gravity* **27**, 173001
(2010). 1324
- [32] D. Eichler, M. Livio, T. Piran, and D. N. Schramm, *Nature
(London)* **340**, 126 (1989). 1325
- [33] R. Narayan, B. Paczynski, and T. Piran, *Astrophys. J. Lett.*
395, L83 (1992). 1326
- [34] R. Mochkovitch, M. Hernanz, J. Isern, and X. Martin,
Nature (London) **361**, 236 (1993). 1327
- [35] S. D. Barthelmy *et al.*, *Nature (London)* **438**, 994 (2005). 1328
- [36] D. B. Fox *et al.*, *Nature (London)* **437**, 845 (2005). 1329
- [37] N. Gehrels *et al.*, *Nature (London)* **437**, 851 (2005). 1330
- [38] M. Shibata, M. D. Duez, Y. T. Liu, S. L. Shapiro, and B. C.
Stephens, *Phys. Rev. Lett.* **96**, 031102 (2006). 1331
- [39] V. Paschalidis, M. Ruiz, and S. L. Shapiro, *Astrophys. J.*
806, L14 (2015). 1332
- [40] N. R. Tanvir, A. J. Levan, A. S. Fruchter, J. Hjorth, R. A.
Hounsell, K. Wiersema, and R. L. Tunnicliffe, *Nature
(London)* **500**, 547 (2013). 1333
- [41] F. Foucart, E. O’Connor, L. Roberts, M. D. Duez, R. Haas,
L. E. Kidder, C. D. Ott, H. P. Pfeiffer, M. A. Scheel, and B.
Szilagyi, *Phys. Rev. D* **91**, 124021 (2015). 1334
- [42] G. Lovelace, M. D. Duez, F. Foucart, L. E. Kidder, H. P.
Pfeiffer, M. A. Scheel, and B. Szilagyi, *Classical Quantum
Gravity* **30**, 135004 (2013). 1335
- [43] M. B. Deaton, M. D. Duez, F. Foucart, E. O’Connor, C. D.
Ott, L. E. Kidder, C. D. Muhlberger, M. A. Scheel, and B.
Szilagyi, *Astrophys. J.* **776**, 47 (2013). 1336
- [44] F. Foucart, *Phys. Rev. D* **86**, 124007 (2012). 1337
- [45] F. Foucart, L. Buchman, M. D. Duez, M. Grudich, L. E.
Kidder, I. MacDonald, A. Mroue, H. P. Pfeiffer, M. A.
Scheel, and B. Szilagyi, *Phys. Rev. D* **88**, 064017 (2013). 1338
- [46] F. Foucart, M. B. Deaton, M. D. Duez, E. O’Connor, C. D.
Ott, R. Haas, L. E. Kidder, H. P. Pfeiffer, M. A. Scheel, and
B. Szilagyi, *Phys. Rev. D* **90**, 024026 (2014). 1339
- [47] M. Shibata and K. Taniguchi, *Phys. Rev. D* **77**, 084015
(2008). 1340
- [48] V. Ferrari, L. Gualtieri, and F. Pannarale, *Phys. Rev. D* **81**,
064026 (2010). 1341
- [49] K. Kawaguchi, K. Kyutoku, H. Nakano, H. Okawa, M.
Shibata, and K. Taniguchi, *Phys. Rev. D* **92**, 024014
(2015). 1342
- [50] B. P. Abbott *et al.* (LIGO Scientific Collaboration, Virgo
Collaboration), *Living Rev. Relativ.* **19**, 1 (2016). 1343
- [51] W. H. Lee and W. L. Kluzniak, *Astrophys. J.* **526**, 178
(1999). 1344
- [52] W. H. Lee and W. L. Kluzniak, *Mon. Not. R. Astron. Soc.*
308, 780 (1999). 1345
- [53] W. H. Lee, *Mon. Not. R. Astron. Soc.* **318**, 606 (2000). 1346
- [54] R. Oechslin, H. T. Janka, and A. Marek, *Astron.
Astrophys.* **467**, 395 (2007). 1347
- [55] J. S. Read, B. D. Lackey, B. J. Owen, and J. L. Friedman,
Phys. Rev. D **79**, 124032 (2009). 1348

- 1381 [56] C. Markakis, J. S. Read, M. Shibata, K. Uryu, J. D. E.
 1382 Creighton, and J. L. Friedman, On recent developments in
 1383 theoretical and experimental general relativity, astrophysics
 1384 and relativistic field theories, in *Proceedings of the 12th*
 1385 *Marcel Grossmann Meeting on General Relativity, Paris,*
 1386 *France, 2009* (2010), Vols. 1–3, pp. 743–745.
- 1387 [57] C. Markakis, J. S. Read, M. Shibata, K. Uryū, J. D. E.
 1388 Creighton, J. L. Friedman, and B. D. Lackey, *J. Phys.*
 1389 *Conf. Ser.* **189**, 012024 (2009).
- 1390 [58] N. Stergioulas, A. Bauswein, K. Zagkouris, and H.-T.
 1391 Janka, *Mon. Not. R. Astron. Soc.* **418**, 427 (2011).
- 1392 [59] W. E. East, F. Pretorius, and B. C. Stephens, *Phys. Rev. D*
 1393 **85**, 124009 (2012).
- 1394 [60] B. D. Lackey and L. Wade, *Phys. Rev. D* **91**, 043002
 1395 (2015).
- 1396 [61] L. Wade, J. D. E. Creighton, E. Ochsner, B. D. Lackey,
 1397 B. F. Farr, T. B. Littenberg, and V. Raymond, *Phys. Rev. D*
 1398 **89**, 103012 (2014).
- 1399 [62] A. Bauswein, N. Stergioulas, and H.-T. Janka, *Phys. Rev.*
 1400 *D* **90**, 023002 (2014).
- 1401 [63] É. É. Flanagan and T. Hinderer, *Phys. Rev. D* **77**, 021502
 1402 (2008).
- 1403 [64] K. Kyutoku, M. Shibata, and K. Taniguchi, *Phys. Rev. D*
 1404 **82**, 044049 (2010).
- 1405 [65] B. D. Lackey, K. Kyutoku, M. Shibata, P. R. Brady, and
 1406 J. L. Friedman, *Phys. Rev. D* **89**, 043009 (2014).
- 1407 [66] F. Pannarale, E. Berti, K. Kyutoku, B. D. Lackey, and
 1408 M. Shibata, *Phys. Rev. D* **92**, 081504 (2015).
- 1409 [67] J. Vines, É. É. Flanagan, and T. Hinderer, *Phys. Rev. D* **83**,
 1410 084051 (2011).
- 1411 [68] A. Maselli, L. Gualtieri, and V. Ferrari, *Phys. Rev. D* **88**,
 1412 104040 (2013).
- 1413 [69] K. Barkett, M. A. Scheel, R. Haas, C. D. Ott, S. Bernuzzi,
 1414 D. A. Brown, B. Szilágyi, J. D. Kaplan, J. Lippuner, C. D.
 1415 Muhlberger, F. Foucart, and M. D. Duez, *Phys. Rev. D* **93**,
 1416 044064 (2016).
- 1417 [70] K. Yagi and N. Yunes, *Phys. Rev. D* **89**, 021303
 1418 (2014).
- 1419 [71] B. D. Lackey, K. Kyutoku, M. Shibata, P. R. Brady, and
 1420 J. L. Friedman, *Phys. Rev. D* **85**, 044061 (2012).
- 1421 [72] M. Vallisneri, *Phys. Rev. D* **77**, 042001 (2008).
- 1422 [73] C. D. Bailyn, R. K. Jain, P. Coppi, and J. A. Orosz,
 1423 *Astrophys. J.* **499**, 367 (1998).
- 1424 [74] V. Kalogera and G. Baym, *Astrophys. J.* **470**, L61
 1425 (1996).
- 1426 [75] L. Kreidberg, C. D. Bailyn, W. M. Farr, and V. Kalogera,
 1427 *Astrophys. J.* **757**, 36 (2012).
- 1428 [76] T. B. Littenberg, B. Farr, S. Coughlin, V. Kalogera, and
 1429 D. E. Holz, *Astrophys. J.* **807**, L24 (2015).
- 1430 [77] R. C. Tolman, *Phys. Rev.* **55**, 364 (1939).
- 1431 [78] J. R. Oppenheimer and G. M. Volkoff, *Phys. Rev.* **55**, 374
 1432 (1939).
- 1433 [79] R. C. Tolman, *Proc. Natl. Acad. Sci. U.S.A.* **20**, 169
 1434 (1934).
- 1435 [80] W. Del Pozzo, T. G. F. Li, M. Agathos, C. Van Den Broeck,
 1436 and S. Vitale, *Phys. Rev. Lett.* **111**, 071101 (2013).
- 1437 [81] J. Abadie *et al.* (LIGO Scientific Collaboration), *Classical*
 1438 *Quantum Gravity* **27**, 173001 (2010).
- 1439 [82] F. Pannarale, E. Berti, K. Kyutoku, B. D. Lackey, and
 1440 M. Shibata, *Phys. Rev. D* **92**, 084050 (2015).
- [83] M. Agathos, J. Meidan, W. D. Pozzo, T. G. F. Li, M. Tompitak, J. Veitch, S. Vitale, and C. V. D. Broeck, *Phys. Rev. D* **92**, 023012 (2015). 1441
- [84] A. Taracchini, Y. Pan, A. Buonanno, E. Barausse, M. Boyle, T. Chu, G. Lovelace, H. P. Pfeiffer, and M. A. Scheel, *Phys. Rev. D* **86**, 024011 (2012). 1442
- [85] A. Buonanno and T. Damour, *Phys. Rev. D* **59**, 084006 (1999). 1443
- [86] A. Taracchini, A. Buonanno, Y. Pan, T. Hinderer, M. Boyle, D. A. Hemberger, L. E. Kidder, G. Lovelace, A. H. Mroue, H. P. Pfeiffer, M. A. Scheel, B. Szilagyi, N. W. Taylor, and A. Zenginoglu, *Phys. Rev. D* **89**, 061502 (2014). 1444
- [87] M. Pürrer, *Phys. Rev. D* **93**, 064041 (2016). 1445
- [88] P. Kumar, K. Barkett, S. Bhagwat, N. Afshari, D. A. Brown, G. Lovelace, M. A. Scheel, and B. Szilágyi, *Phys. Rev. D* **92**, 102001 (2015). 1446
- [89] P. Kumar, T. Chu, H. Fong, H. P. Pfeiffer, M. Boyle, D. A. Hemberger, L. E. Kidder, M. A. Scheel, and B. Szilagyi, *Phys. Rev. D* **93**, 104050 (2016). 1447
- [90] LIGO Scientific Collaboration, LSC Algorithm Library software packages LAL, LALWRAPPER, and LALAPPS. 1448
- [91] M. Pürrer, M. Hannam, and F. Ohme, *Phys. Rev. D* **93**, 084042 (2016). 1449
- [92] D. Foreman-Mackey, D. W. Hogg, D. Lang, and J. Goodman, *Publ. Astron. Soc. Pac.* **125**, 306 (2013). 1450
- [93] A. Gelman and D. B. Rubin, *Stat. Sci.* **7**, 457 (1992). 1451
- [94] B. S. Sathyaprakash and B. F. Schutz, *Living Rev. Relativ.* **12**, 2 (2009). 1452
- [95] F. Foucart, M. D. Duez, L. E. Kidder, M. A. Scheel, B. Szilágyi, and S. A. Teukolsky, *Phys. Rev. D* **85**, 044015 (2012). 1453
- [96] F. Pannarale, L. Rezzolla, F. Ohme, and J. S. Read, *Phys. Rev. D* **84**, 104017 (2011). 1454
- [97] M. Puerrer *et al.* (to be published). 1455
- [98] B. Kiziltan, A. Kottas, M. De Yoreo, and S. E. Thorsett, *Astrophys. J.* **778**, 66 (2013). 1456
- [99] I. Mandel, *Phys. Rev. D* **81**, 084029 (2010). 1457
- [100] K. Chatzioannou, K. Yagi, A. Klein, N. Cornish, and N. Yunes, *Phys. Rev. D* **92**, 104008 (2015). 1458
- [101] B. P. Abbott *et al.* (Virgo, LIGO Scientific), *Phys. Rev. Lett.* **116**, 061102 (2016). 1459
- [102] B. P. Abbott *et al.* (Virgo, LIGO Scientific), *Phys. Rev. Lett.* **116**, 241103 (2016). 1460
- [103] B. P. Abbott *et al.* (Virgo, LIGO Scientific), *Astrophys. J.* **832**, L21 (2016). 1461
- [104] J. Abadie, B. P. Abbott, R. Abbott, T. D. Abbott, M. Abernathy, T. Accadia, F. Acernese, C. Adams, R. Adhikari, C. Affeldt *et al.*, *Astron. Astrophys.* **541**, A155 (2012). 1462
- [105] L. P. Singer *et al.*, *Astrophys. J.* **795**, 105 (2014). 1463
- [106] L. P. Singer and L. R. Price, *Phys. Rev. D* **93**, 024013 (2016). 1464
- [107] C. Pankow, P. Brady, E. Ochsner, and R. O’Shaughnessy, *Phys. Rev. D* **92**, 023002 (2015). 1465
- [108] B. P. Abbott *et al.* (InterPlanetary Network, DES, INTEGRAL, La Silla-QUEST Survey, MWA, Fermi-LAT, J-GEM, DEC, GRAWITA, Pi of the Sky, Fermi GBM, MASTER, Swift, iPTF, VISTA, ASKAP, SkyMapper, PESSTO, TOROS, Pan-STARRS, Virgo, Liverpool 1466
- [109] 1467
- [110] 1468
- [111] 1469
- [112] 1470
- [113] 1471
- [114] 1472
- [115] 1473
- [116] 1474
- [117] 1475
- [118] 1476
- [119] 1477
- [120] 1478
- [121] 1479
- [122] 1480
- [123] 1481
- [124] 1482
- [125] 1483
- [126] 1484
- [127] 1485
- [128] 1486
- [129] 1487
- [130] 1488
- [131] 1489
- [132] 1490
- [133] 1491
- [134] 1492
- [135] 1493
- [136] 1494
- [137] 1495
- [138] 1496
- [139] 1497
- [140] 1498
- [141] 1499
- [142] 1500

- 1501 Telescope, BOOTES, LIGO Scientific, LOFAR, C2PU,
1502 MAXI), *Astrophys. J.* **826**, L13 (2016).
- 1503 [109] F. Foucart, M. B. Deaton, M. D. Duez, L. E. Kidder, I.
1504 MacDonald, C. D. Ott, H. P. Pfeiffer, M. A. Scheel, B.
1505 Szilagyi, and S. A. Teukolsky, *Phys. Rev. D* **87**, 084006
1506 (2013).
- [110] T. Hinderer *et al.*, *Phys. Rev. Lett.* **116**, 181101
1507 (2016).
- [111] L. Santamaría, F. Ohme, P. Ajith, B. Brügmann, N.
1508 Dorband, M. Hannam, S. Husa, P. Mösta, D. Pollney,
1509 C. Reisswig, E. L. Robinson, J. Seiler, and B. Krishnan,
1510 *Phys. Rev. D* **82**, 064016 (2010).
- 1511 1512
- 1513